Satellite remote sensing of river discharge: a framework for assessing the accuracy of discharge estimates made from satellite remote sensing observations

David Bjerklie[a,*] **Michael Durand**[b] **James Lenoir**[a] **Robert W. Dudley**[a] **Charon Birkett**[c] **John W. Jones**[d] **and Merritt Harlan**[d]

[a]U.S. Geological Survey New England Water Science Center, Northborough, Massachusetts, United States
[b]Ohio State University, Columbus, Ohio, United States
[c]NASA Goddard Space Flight Center, Greenbelt, Maryland, United States
[d]U.S. Geological Survey Hydrologic Remote Sensing Branch, Kearneysville, West Virginia, United States

Abstract. This research presents an evaluation of the accuracy and uncertainty of estimates of river discharge made using satellite observed data sources as input to a modified form of Manning's equation. Conventional U.S. Geological Survey (USGS) streamflow gaging station data and *in-situ* measurements of width, depth, height, slope, discharge, and velocity from 30 USGS gage sites were used as ground-truth to assess accuracy. This study explores accuracy in relation to the amount of ground truth information available, the number of calibration points available, and the accuracy of the input data. This research indicates that remotely sensed discharge estimates associated with the modified Manning equation may be expected to have an uncertainty in range of 10% overall given a sufficient number of calibration points. The uncertainty associated with the modified Manning algorithm increased markedly for depths <3 meters (m) and for discharges <1000 cubic meters per second (m^3/s) for many rivers after calibration. Rivers that exhibit (1) a wide range of flow conditions, (2) a significant number of dams in the watershed and along the channel, and (3) a high baseflow index are more likely to have relatively large errors overall and particularly at the low end of the streamflow range. Uncertainty in remotely sensed measurements of water-surface elevation (WSE) and width in the expected range (WSE, $+/-10$ cm; Width, $+/-15$ m) introduces uncertainty in the discharge estimates on the order of 10% and is greatest at the low end of discharge as rivers get shallower and narrower. As WSE and width measurement uncertainty increases, discharge uncertainty increases accordingly. In general, the observation errors are greater than the errors associated with the algorithm for a well-calibrated model (e.g., 20 calibration points). [DOI: 10.1117/1.JRS.17.014520]

Keywords: river discharge; satellite remote sensing; uncertainty.

Paper 220551G received Sep. 21, 2022; accepted for publication Mar. 3, 2023; published online Mar. 28, 2023.

1 Introduction

There has been considerable interest in recent years in using observations from remote platforms to observe and track water fluxes in rivers on a global scale. The U.S. Geological Survey (USGS), National Aeronautics and Space Administration (NASA), and other agencies around the world are working toward using satellite observations of water-surface height and width, often combined with hydrologic and hydraulic modeling, to estimate discharge in rivers independent of permanent ground-based streamgages. Additionally, remote sensing of river height, width, and discharge could contribute considerably to the calibration and validation of hydrologic models.[1,2] The NASA Surface Water and Ocean Topography mission (SWOT), which was

*Address all correspondence to David Bjerklie, dmbjerkl@usgs.gov

launched in December 2022, will provide unprecedented observational coverage of water surface widths, heights, and slopes in rivers, lakes, and wetlands across the globe with repeat observations of 21 days or less.[3,4]

Uncertainties arise from the type of flow model used to compute discharge, the ability to predict the parameters of that model, and the uncertainties in the observational data used in the model. Uncertainties associated with conventional ground-based discharge gaging stations, which correlate water-surface elevation (WSE) with discharge (Q), have been assessed by Kiang et al.[5] In general, they observed that even with robust calibration, the assumption that there is a one-to-one (monotonic or kinematic) relation between water level and discharge results in some uncertainty. Kiang et al.[5] also considered the effect of smoothing to construct a kinematic rating curve between WSE and Q on overall uncertainty in the estimates of Q.

Recent efforts have accelerated the diversification of approaches for estimating discharge from remote platforms due to improvements in satellite sensors (both radars and optical) that observe water bodies more accurately with increased spatial and temporal coverage. The importance of understanding the uncertainty for both uncalibrated and partly calibrated (using prior information) methods is considered for algorithms used to translate remote observations to discharge. For example, Gleason and Smith[6] showed that observations of width alone, in the context of reach scale hydraulic geometry, can be used to estimate discharge with <30% root mean squared error (RMSE) in a number of rivers.

Birkinshaw et al.[7,8] demonstrated that satellite-derived WSE (stage), slope, and width can be used to estimate discharge between gaged locations when the gage discharge is a boundary condition, or a suitable reference depth is derived from limited discharge information. Durand et al.[9] used inverse modeling techniques to estimate discharge in the River Severn, United Kingdom, via a physically-based flow resistance equation with initial estimates of the unknown parameters, including bottom depth and a flow resistance coefficient. Similarly, Garambois and Monnier[10] applied inverse methods and remote observations of river surface features to estimate various hydraulic properties of the river flow in the Garonne River, France. Both methods produced estimates within 15% of observed discharge for the particular river of interest.

Further investigations by Durand et al.[11] and Bonnema et al.[12] incorporated modeled river data as a proxy for satellite observations to test various uncalibrated physically-based and quasi-physically-based discharge algorithms in a set of rivers in the United States and France, and in the Ganges-Brahmaputra, India. They included modeled water-surface area of the river to provide a reach average width, and the stage for the water-surface along the reach to provide surface slope and change in flow depth. The discharge algorithms tested in Durand et al.[11] and Bonnema et al.[12] vary in accuracy depending on river and reach, and the results were within about 10% RMSE in some cases. A more extensive application of an uncalibrated remote sensing-based width-discharge rating algorithm, where width is estimated from Landsat and is calibrated with modeled river discharge estimates, was tested against 456 ground-based gaging stations,[13] finding a median Kling–Gupta efficiencies (KGEs) of 0.3.

The previous discussion focused on studies that estimated discharge with little or no calibration of the algorithm parameters; however, the test cases were limited primarily to a small set of modeled river discharge and in some cases used prior information on the state of the river to provide partial calibration. Frasson et al.,[14] evaluated sources of error and the expected accuracy of SWOT-based estimates of discharge, concluding that the primary sources of error come from parameter uncertainty in the discharge algorithm and that these uncertainties are linked to hydraulic and geomorphologic variability and bias associated with prior information used to constrain the estimates. Bjerklie et al.[15] estimated discharge in the Yukon River at two locations in Alaska using only observations of the river channel with mean accuracy better than 20% without calibration and better than 5% with calibration, indicating that the simplified flow law (discharge equation) central to the algorithm had an accuracy on the order of 5%. Additionally, this analysis does not address overbank (flood) discharge estimates. Overbank flow is often defined by complex landscapes that might include urban, forest, wetland, meadows, and agricultural lands, as well as combined level and steep mountain terrain. As such, the difficulty of evaluating and estimating flow during floods may be increased considerably and is of necessity left as a separate future study.

Satellite remote sensing of the water surface height, width, and slope of rivers enables extensive spatial coverage across the globe and the possibility of dense temporal coverage through

the use of multiple satellite platforms. Given the global spatial coverage as many as 200,000 river reaches will be observed (SWOT River Products | NASA SWOT). However, only a small fraction of these rivers will have ground-based gaging stations that can be used to calibrate the observations to estimate discharge, indicating that extensive river discharge estimates from the majority of river reaches will not have the luxury of calibration measurements and will effectively have an unknown accuracy. This paper presents a review of the accuracy of a calibrated model that is based on a generalized flow resistance model for a range of rivers that is independent of limitations of satellite observations and prior hydrologic information.[16] This is accomplished by assuming a best-case scenario where ground measurements are available, leaving model accuracy as the primary component of expected error. Additionally, the calibrated models provide a glimpse into the range of error that might be expected across varying river size, morphology, and hydrologic setting such that inferences might be made at similar uncalibrated locations.

The limited studies conducted to date provide some indication of the accuracy that might be expected from remote sensing-based estimates of discharge. However, the general accuracy parsed according to the sources of error and evaluation of the error distribution across the range of discharge for a large number of rivers has not been undertaken and is not currently understood. A robust assessment of the accuracy includes those of the observations themselves, the supporting information and modeling assumptions, and the parameters used in the algorithm. Additionally, it is imperative to understand how error varies across the entire flow regime to aid in application of the remote sensing-based estimates.

The accuracy of remote sensing discharge (RSQ) estimates for any given river reach can only be assessed relative to discharge and other hydraulic information directly measured or developed from a conventional ground-based streamgaging rating curve (i.e. "ground-truth") despite acknowledged uncertainties with these measurements.[5,17] Ideally, such an assessment would use enough ground-truth information to provide a reasonable estimate of accuracy that would be expected to hold for future estimates provided conditions do not change significantly. In the case of remote sensing of discharge, the ability to assess accuracy from ground truth for most river reaches where estimates are being made is not possible due to the large number of river reaches being observed compared to the number of streamgages where ground-truth data are available. Complicating the assessment of accuracy is the fact that it may vary depending on the magnitude of flow being estimated—the accuracy at low flows may be quite different than the accuracy for mean flow, higher flows, and especially overbank floods. Additionally, the accuracy of the ground-truth data may be important to consider. For most cases, ground-truth data sets derived from hydraulic models pose additional potential for increased uncertainty and require an evaluation of the parameters used to calibrate them.[11]

This paper evaluates the accuracy and limitations of the same flow law used by Bjerklie et al.[15] but for a larger set of rivers. The analysis is designed to evaluate uncertainty due to the limitations of the discharge flow law (modified Manning equation) separately from the uncertainty of the measurements used in computing river discharge using satellite (and other) remotely observed data sources (RSQ). Conventional USGS streamflow gaging station data and direct measurements of width, depth, height, slope, discharge, and velocity from 30 USGS gage sites were used as ground-truth to assess accuracy (Table 1). This study also explored accuracy in relation to the amount of ground truth information available for comparison as well as examination of factors known to improve the expected accuracy including the river morphology, the number of calibration data available, and the accuracy of the input data.

1.1 *Background*

Observations of river dynamics from remote (satellites, aerial, and bankside) platforms involve the direct measurement of water-surface area, which when divided by reach length yields reach-averaged width, as well as the WSE (or stage) along the reach (relative to a known datum). These measurements are made either at a prescribed section (in the case of bankside or aerial mounted instruments, or satellite nadir tracks) or as a reach average (in the case of satellite or aerial mounted swath instruments). Reach measurements of water-surface height can also yield water-surface slope. Observations of width and height are currently being measured routinely

Table 1 USGS Streamflow Gaging Stations used in this study along with gaging reach morphology and hydrologic information obtained from Frasson et al.[18,19] (Variable definitions in Frasson et al.[18,19]).

Station number	River name	Number of discharge measurements used for analysis	Water-surface slope	Meander wavelength of gaged reach (m)	Sinuosity of gaged reach	Average width in meander of gaged reach (m)	Mean annual flow estimate at gage (m^3/s)	Stream power normalized by width (W/m)
01184000	Connecticut River at Thompsonville, CT.	57	0.00026	1745.00	1.06	338.17	392.55	1016.06
01434000	Delaware River at Port Jervis, NY	158	0.00106	3385.32	1.27	144.05	91.26	942.08
01515000	Susquehanna River near Waverly, NY	115	0.00048	4845.10	1.07	115.79	199.49	938.62
01576000	Susquehanna River at Marietta, PA	50	0.00048	4116.26	1.25	701.43	716.88	3381.54
01638500	Potomac River at Point of Rocks, MD	152	0.00029	3326.40	1.02	249.18	219.25	612.87
02087500	Neuse River near Clayton, NC	159	0.00031	1688.23	1.37	37.68	19.35	58.24
02129000	Pee Dee R NR Rockingham, NC	153	0.00019	3362.59	1.07	259.59	2.55	4.76
03593500	Tennessee River at Savannah, TN	41	0.00005					
05082500	Red River of the North at Grand Forks, ND	111	0.00007	1475.02	1.01	80.68	58.36	40.59
06185500	Missouri River near Culbertson, MT	130	0.00016	6925.09	1.45	279.87	80.63	126.11
6820500	Platte River near Agency, MO	144	0.00028					
06934500	Missouri River at Hermann, MO	120	0.00018	7406.40	1.02	491.03	17927.15	31469.47
7020500	Mississippi River at Chester, IL	122	0.00007	4882.58	1.01	632.72	25263.70	18303.61
07022000	Mississippi River at Thebes, IL	126	0.00007	6187.58	1.04	677.23	25431.42	17042.33
9261000	Green River near Jensen, UT	159	0.00233	1400.71	1.89	71.05	26.38	602.14
11377100	Sacramento R AB Bend Bridge NR Red Bluff, CA	157	0.00068	1025.35	1.00	71.86	265.23	1754.38
11389500	Sacramento R A Colusa, CA	143	0.00013	931.45	1.02	73.80	377.00	461.27

Table 1 (*Continued*).

Station number	River name	Number of discharge measurements used for analysis	Water-surface slope	Meander wavelength of gaged reach (m)	Sinuosity of gaged reach	Average width in meander of gaged reach (m)	Mean annual flow estimate at gage (m^3/s)	Stream power normalized by width (W/m)
12150800	Snohomish River near Monroe, WA	148	0.00010	1851.04	1.00	91.09	150.88	143.65
12399500	Columbia River at International Boundary	92	0.00023	1512.76	1.06	237.13	1365.13	3010.15
12422500	Spokane River at Spokane, WA	93	0.00227	928.43	1.04	46.40	96.85	2149.81
12462500	Wenatchee River at Monitor, WA	133	0.00305					
14191000	Willamette River at Salem, OR	81	0.00028	3657.72	1.10	173.06	495.33	1352.13
15304000	Kuskokwim R at Crooked Creek, AK	127	0.00013					
15356000	Yukon R at Eagle, AK	86	0.00020					
15453500	Yukon R NR Stevens Village, AK	36	0.00009					
15485500	Tanana R at Fairbanks, Ak	86	0.00043					
15515500	Tanana R at Nenana, AK	56	0.00057					
15565447	Yukon R at Pilot Station, AK	124	0.00003					
15875000	Colville R at Umiat, AK	114	0.00047					
15908000	Sagavanirktok R NR Pump STA 3, AK	70	0.00305					
	Mean		0.00060	3192.27	1.14	251.15	3851.55	4389.99
	stdev		0.00087	2074.65	0.22	219.87	8588.33	8444.06
	max		0.00305	7406.40	1.89	701.43	25431.42	31469.47
	min		0.00003	928.43	1.00	37.68	2.55	4.76

from various imaging and nadir pointing altimetric satellites, although not concurrently. The NASA/CNES/CSA/UKSA SWOT wide-swath altimeter mission launched December 2022,[4] will concurrently measure both water-surface width, height, and slope. Fujita et al.,[20] Kääb et al.,[21] and Legleiter and Kinzel[22] have demonstrated that surface velocity in some rivers can be measured from satellite platforms by tracking ice floes and turbulent irregularities in the flow, however, widespread routine measurements of velocity from satellites are not expected in the near future.

The tracking of river dynamics and discharge from remote platforms rely on width and stage observations, coupled with limited *in-situ* (ground-based) observations to develop time-series data with intervals between observations on the scale of days to weeks.[23–32] More recently, Refs. 9, 11, and 12 have developed discharge algorithms designed to apply observations of width, stage, and slope observations from the SWOT mission. Limited field observations provide ground truth information for calibration and accuracy assessment of remotely sensed estimates of discharge (RSQ). Alternatively, modeled river flows also may serve as points of calibration (for example from global hydrologic models as reported in the global reach-scale *a-priori* discharge estimates for SWOT (GRADES) website.[33]

The selection of the river reach is an important consideration in the accuracy and uncertainty of remote sensing-based discharge estimates because of the role the geometry of the channel reach plays in the energy slope and in the flow resistance. The measurement data used in this study were all collected at individual cross-sections within a reach that is not defined. As such, the reach characteristics are not included as part of the evaluation. In many remote sensing-based applications to rivers, the river reach is also not considered because it is defined by the orbital crossings rather than by physical attributes of the reach. In any case, Frasson et al.[16] have shown that over longer reaches (5 to 15 km) errors in satellite observed width, height, and slope are reduced, indicating that over these reach lengths, estimate accuracy is likely to be better than over shorter reaches. Additionally, channel morphology characteristics that reflect river hydraulic conditions[24,34] can better be defined over longer reaches.

The goal of the RSQ methodology presented in this paper is to estimate discharge using an approach that incorporates the use of *in-situ* information as much as practicable. Even small amounts of *in-situ* information can provide the means to constrain unknown parameters to minimize the degrees of freedom available for calibration. RSQ estimates presented herein are developed for in-bank flow conditions and strive to represent the mean hydraulic conditions in the channel (mean depth and velocity). Overbank flood flow accuracy is not addressed.

Inherent limitations in flow-law-based discharge estimation methods include the use of a continuous representation of flow resistance within a flow resistance equation such as the Manning equation. These methods rely on the assumption that flow resistance is a linear function of observed variables and that the flow is contained within a defined channel. Additionally, the remote discharge estimates are limited to in-bank flow, periods of no ice cover and obstructing clouds, and to river widths >50 m if using satellite imagery. The observational record is also constrained by the revisit period and the distance between the ground paths traced out by the satellite orbit. These latter two limitations in most cases will limit repeat observations to several days and several kilometers (km) at best. These constraints require that the discharge estimates are independent of one another, and therefore do not assume continuity between observations in time or space and do not rely on transient or routing-based flow computations.

The remote sensing capabilities include observations of the river width and the river height. Validation studies for both observed variables have been conducted at many locations using different instruments mounted on various satellite platforms[25–27,31,35–42] and these have provided first-order expected observations accuracies. Along with these studies, the spatial (x, y, and z coordinates) accuracies are generally reported based on the specifications of the observing instruments, including discussion of factors that may reduce accuracy. Recently, observations of water-surface height in rivers (and other water bodies) derived from the multi-agency Jason-2 and Jason-3 satellite altimeter missions provide an estimate of observational error. These estimates are based on qualitative characteristics of the target as well as atmospheric and instrument conditions and responses. As such, they are not precise errors but rather are a first order of an expected error that is quantitative, based on characteristics of the observation.[43]

1.2 *Ground Truth Data*

The ground truth information used to evaluate the remote sensing estimates includes direct measurements of discharge, water-surface height, water velocity, and water depth in river cross-sections, and the rating curve produced by relating the measured water-surface height to the discharge. These direct measurements are considered to be the best available truth set with the following qualifiers and caveats.

Measurement of water-surface height at USGS streamgages adheres to a rigorous accuracy standard (0.3 cm).[44] When ice is covering the water-surface, stage may be affected and ice corrections applied. Water velocity and depth in the cross-section is measured using acoustic doppler current profiler (ADCP) technology in most cases. The accuracy of these measurements depends on the operation checks on the equipment, flow conditions during the measurement, and operator skill. The depth and velocity measurements are made across the channel in a more or less continuous flow field, with width measured perpendicular to the direction of flow. The measurement accounts for lateral and vertical flow to derive a mean flow in the downstream direction.

The discharge is computed from the velocity-depth flow field as the product of mean depth, velocity, and width. The USGS rates the discharge measured as poor, fair, good, or excellent based on the quality of the measurement conditions and equipment operation. In general, it is assumed that a poor measurement has an accuracy that is >8% of the "actual" discharge, a fair measurement within 8%, a good measurement within 5%, and an excellent measurement within 2%.[45] However, inherent errors in the measurements are not considered in this study as part of the uncertainty in the remote sensing estimates of discharge.

2 Uncertainty Associated with Remote Sensing-Based Discharge Estimates

There are three types of error or uncertainty that contribute to the overall error of any given remote sensing-based discharge estimate using the methods developed in this study. Yoon et al.[46] and Tuozzolo et al.[47] have assessed the error (uncertainty) associated with large-scale applications of various remote sensing-based discharge estimation algorithms. These include

1. **Algorithm approximation uncertainty**: This error is associated with the assumptions in, and the applicability of the flow law (or algorithm) used to predict discharge if perfect observations were available. This error may also include error in estimates of other hydraulic characteristics of the flow including depth and velocity. The error associated with assumptions within the algorithm may vary and may not be the same across the entire range of flow.
2. **Observation uncertainty:** This consists of error associated with observations of the water-surface height, the water-surface width, and the water-surface slope.
3. **Algorithm parameter uncertainty:** This is the error associated with the values used as constant parameters in the algorithm and includes those that define the flow resistance in the channel and the depth in the channel. For cases where discharges are available to calibrate against, this uncertainty is relatively small. For cases where algorithms such as mass-conserved flow law inversion are used, parameter uncertainty dominates.

2.1 *River Discharge Algorithm Development and Uncertainty*

The algorithm specifically evaluated here was developed by the USGS to estimate discharge remotely and is based on the Manning equation. [48] There are similar algorithms that have been developed that do not require calibration but rather enforce mass conservation based on the Manning equation and on hydraulic geometry principles.[49,50] The Manning equation is an empirical adaptation of the Chezy equation, which describes a state of uniform flow that is neither accelerating nor decelerating but is maintained at a steady rate (mean velocity remains constant in the reach).

The Chezy equation is given as

$$V = C\sqrt{\mathrm{RS}}, \tag{1}$$

and the Manning equation

$$V = \frac{R^{0.67}S^{0.5}}{n}, \tag{2}$$

where V is the mean velocity of flow (m/s); R is the hydraulic radius of the flow (flow area divided by the wetted perimeter) (m); S is the energy slope (taken as the water-surface slope in many cases); C is the Chezy coefficient (index to flow resistance); and n is the Manning resistance coefficient

Refer to the Appendix for the conceptual development of these equations.

Both the Manning and the Chezy equations provide estimates of the mean velocity in the channel (V), and when multiplied by the cross-sectional area of the channel (top width, W, times the mean depth, Y) yield the discharge, Q. The hydraulic radius, R, is approximately equal to Y within $+/-10\%$ or less for rivers with width to depth ratios >18 for rectangular channels[51] and for parabolic channels this can be demonstrated for channels with width to depth ratios >10. Many rivers[52] have width to depth ratios >20, which for parabolic shapes means the difference between the hydraulic radius and the mean depth is $<5\%$. Similarly, Bjerklie et al.[26] have shown that from a practical perspective, the water-surface slope yields similar statistics when used in the Manning equation compared to the energy slope for a wide range of rivers. As such, for application purposes, the water-surface slope is equivalent to the energy slope (S) given that the water-surface slope can be directly measured.

The Chezy equation is derived from the principle that the source of flow resistance via shear stress on the channel boundary (the bed and banks) is viscous friction. However, in practice, flow resistance in rivers includes a number of interactions that expend energy and contribute to flow resistance. Additionally, energy loss is associated with irregular channel geometry and flow conditions, bedload transport, turbulent lateral and vertical motion in the flow field, form drag around large obstacles (e.g., boulders and fallen trees on the channel bottom), and shallow water wave resistance.[53,54] The modification of the Chezy equation by Manning, in effect, describes some of the energy loss as a function of the depth (hence the exponent 0.67 rather than 0.5). Bjerklie[24] also has shown that some portion of the flow resistance is a function of slope and can account for some flow variance in rivers assuming a slope exponent of 0.33 rather than 0.5. The result of the modification by Manning to include a depth exponent of 0.67 renders the Manning coefficient and thus the Manning equation itself a semi-empirical flow law. Thus, the Manning flow resistance coefficient becomes an empirical loss coefficient that accounts for any and all forms of energy loss in the flow, with the caveat that some of that energy loss is already accounted for by the modification of the depth exponent.

The Chezy equation may be considered to be based on physical principles provided it is accepted that the shear stress is a function of velocity squared per Eq. (1). Fundamental assumptions of the equation – or any flow resistance equation – are that the slope and resistance are primarily a function of the channel topography and boundary. The Manning equation indicates that the Chezy resistance coefficient is not constant in a river reach and is not purely a function of the boundary shear stress but is dependent on the depth to the one-sixth power, resulting in the exponent on the hydraulic radius being raised to the two-third power rather than a half. This improvement in flow prediction at varying depths using Manning as opposed to Chezy is demonstrated by Bjerklie et al.[25] As such, we can state that using the Chezy equation to compute flow at any given flow level can be assumed to be physically based and free of model error provided the width and mean depth of the channel are accurately known, and the mean velocity is computed accurately via a known Chezy resistance coefficient. However, the Manning equation has an implicit assumption that flow resistance is related to the hydraulic radius, which imparts non-dimensional homogeneity and therefore possible error due to the assumption.

Given the wider application of the Manning equation, we can assume that it also can be considered free of error for a given flow level provided the width, mean depth, and manning resistance coefficient are accurately known. However, due to the application of Manning at

varying flow levels, even given the improvement rendered in its more general application due to relating the resistance to change in depth to the one-sixth power, we cannot argue that the Manning is a physically based formula for all flow levels due to the uncertainty and empirical nature of defining the flow resistance (the Manning n).

Remote observations provide measurements of the channel top width, water-surface height (and thus the change in depth), and the water-surface slope. As a consequence, the water-surface slope becomes the proxy for the friction slope that is the basis for the Manning and Chezy equation formulations, and some error is associated with this assumption. Bjerklie et al.[26] have shown that using an average slope over the range of flows in a wide range of rivers causes minimal change in discharge estimates compared to using a dynamic slope. Based on this, we might assume that using the water-surface slope rather than the friction slope would also have minimal impact under most natural conditions.

While remote observations provide river water-surface heights, without a way to measure the channel bottom height to translate the water-surface height to a mean channel depth, an assumption must be made regarding the shape of the channel cross-section. Bjerklie et al.[55] have shown that for thousands of rivers over a large range in discharge, the ratio of the maximum to the mean depth in a river is close to 1.5, which is the ratio that would result if the typical cross-section were parabolic. An assumed parabolic cross-section shape allows for a linear relationship between the width squared and the height observations to be extrapolated to a bottom height or elevation of zero flow (represented by the y-intercept of the height as a function of the width). Similarly, the assumption of a parabolic shape allows for the height change to be converted to a mean depth by dividing the height change by 1.5. The error associated with the assumption of a max-to-mean depth ratio of 1.5 can be inferred from the statistics elaborated by Bjerklie et al.[55]

As previously mentioned, given the nature of flow in natural channels, the flow resistance coefficient is also associated with backwater effects due to the contraction and expansion of flow and changes in cross-section,[56–59] submerged obstructions, channel curvature,[24,51,60–64] sediment load,[58] and changes in boundary roughness along the reach and with changing depth. Factors affecting changes in flow resistance with depth include sediment sorting, occurrence of bedrock, presence of sand and cobble bars, presence of vegetation, etc.[58]

Because of the complexity of natural rivers, a constant value for the Manning flow resistance (n) under all flow conditions in a river reach would be an unrealistic assumption.[25,57,58,65] Numerous studies have shown that the Manning n in most rivers varies with depth at a point and spatially within the reach. In addition, the Manning n can vary significantly between rivers and in a downstream direction. Several studies have shown that the bankfull Manning n is related to the channel slope and that the Manning n can be modeled as a logarithmic or power function of the relative depth (diminishing with increasing depth[15,51,58,66]). Given the empirical and highly variable nature of Manning n in any given river, the independent assessment of accuracy in its estimation for all flow levels cannot be realistically accomplished. However, the bankfull or high flow estimate of its value may be compared to literature values and the many flood studies conducted by the USGS and others.

The model framework (algorithm) we present for computing discharge from remote sensing observations is based on a modified form of the Manning equation with a calibratable Manning n function continuous over the range of flows (i.e., no discontinuities in channel configuration of roughness elements) coupled with the assumption of a regular cross-section geometry as indicated by Bjerklie et al.[55] The application of this equation is based on the following general assumptions—the slope and resistance are primarily a function of the channel topography and boundary, and flow resistance can be modeled as a continuous function of depth. It is also assumed that the stage has a monotonic relation to both width and discharge. The application of the parabolic assumption to the river cross-section also has an unknown independent impact on the discharge estimate but is assumed to be minor (see Sec. 2.2.1 following). The Manning equation model used for estimating discharge is parsed to be able to uniquely estimate the Manning roughness coefficient:[15]

$$Q = \frac{\left[W * \left((h-B) * \left(1 - \left(\frac{1}{1+r}\right)\right)\right)^{1.67} * S^{0.5}\right]}{n}, \tag{3}$$

where Q is the river discharge, (m^3/s); W is the width of flow, (m); h is the water-surface height above a common datum, (m); S is the water-surface slope; n is the Manning roughness (resistance) coefficient; B is the height of zero flow, (m); and r is the assumed channel shape coefficient = 2 for a parabolic cross-section shape.

The value of the Manning n is calibrated based on a conceptual relative depth relation that is represented by an assumed power law relation.[51,58,66] The relative depth is formulated between the bankfull depth and the flow depth at the time of the observation multiplied by the baseline Manning n at bankfull depth, assuming that the Manning n at bankfull is at its lowest value.[57,64,65,67] This relation is given as[15]

$$n = n_b * \left(\frac{H - B}{h - B}\right)^x, \tag{4}$$

where n_b is the bankfull reference flow resistance (Manning n) and H is the bankfull height. The value of x, the exponent of the Manning n function given by Eq. (4), is calibrated for flows within bank and can also be calibrated for separate sections of the flow rating to derive a compound rating curve for the reach. A positive value for x implies that flow resistance decreases with increasing depth. For overbank flows, a separate Manning n function can be calibrated if enough overbank flow data are available. As a simple approach for overbank flow, the sign of x can be reversed such Manning resistance will increase as depth increases above bankfull. However, overbank flow uncertainty is not evaluated in this study due to the increased complexity and lack of sufficient overbank flow measurements for calibration.

The Manning equation can be calibrated to any continuous monotonic distribution of discharge values in a river provided the Manning n can vary to match the discharge given the physical structure of the equation is fixed—meaning the depth and slope exponents are constant. However, given that the Manning n will not (and cannot) be calibrated to each individual discharge, a continuous Manning n function, as shown for Eq. (4) above, must be used. The form of the Manning n function will constrain how well the Manning n will match each discharge estimate and will not be able to account for variation beyond the limits of the function.

2.1.1 *Testing the discharge algorithm*

Information from a set of flow measurements was assembled to test the application of the discharge algorithm derived in the previous section. A sample of USGS flow measurement data was downloaded from USGS National Water Information System (NWIS) database[68] from gaging stations on 30 rivers in the United States (Fig. 1). The rivers were selected to provide a range of

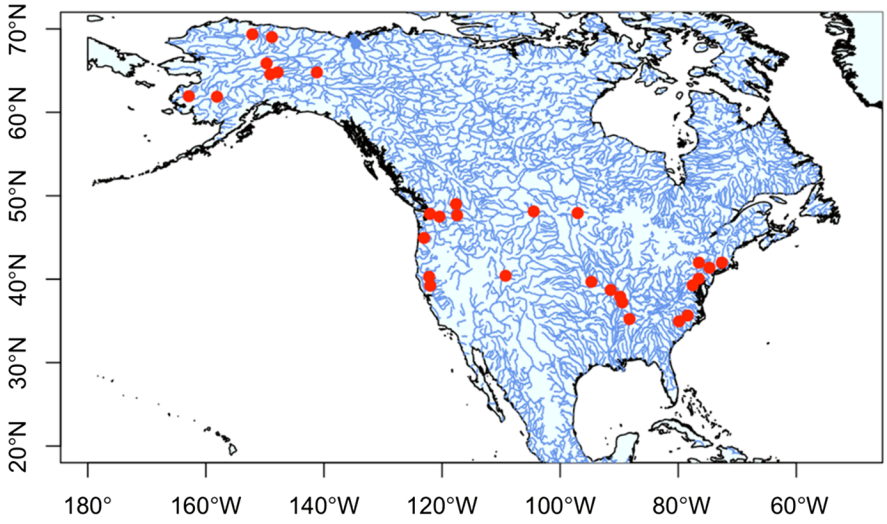

Fig. 1 Map showing location of 30 USGS streamgages used to develop the 30-river discharge data set.

geographic locales and sizes of rivers, with all widths greater than 30 m (i.e., a minimum size putatively observable by spaceborne instruments). The measurement data were supplemented with water-surface slope and other geomorphologic information and assumed to represent ground truth. The data set was composed of 37 to 160 USGS discharge measurements from each of 30 gaged rivers, chosen to be geomorphologically and geographically diverse across the United States, with eight rivers located in Alaska (Table 1). The measurements include the height of the water-surface stage for a specific location, the measured water-surface width, mean depth, mean velocity, and the discharge computed from width times depth times velocity. The width, depth, and velocity data were measured at cross-section locations that vary in the gaged reaches, and as such do not necessarily represent the reach averaged quantities that will be observed remotely. To address this, a quality control process was implemented that includes a rule that the width and stage must correlate positively and vary monotonically.

For the purposes of this study, the maximum measured stage and depth are considered representative of the bankfull state. Information on river channel physical characteristics was also collected for each stream gage including the slope, meander length, sinuosity of the reach containing the gage, Landsat measured width, and modeled mean and 2-year discharge.[69] The characteristic data were obtained from Frasson et al.[18,19] or were independently measured by the USGS or obtained from available Geographic Information System (GIS) sources. These data and sources are reported in LeNoir et al.[69] The data were selected without consideration of the distribution of flow duration such that moderate to low flows are likely over-represented relative to high flows in frequency of measurement.

2.1.2 *Quality control of the discharge data*

Quality control requirements were applied to the flow measurements to ensure the representativeness of the data. The primary screening criteria required that the reported discharge within 5% of the discharge as calculated by multiplying the reported width, depth, and velocity. Additional quality control requirements are itemized below; data that failed any single screening criterion were censored from the record:

1. The width-stage relation reasonably represents a relation where a unique width is associated with a unique stage (monotonic) and the width and stage both increase in the same direction (positive correlation) at different rates, often as a power law. This requirement considers some normal random scatter around a general monotonic trend that can be smoothed by fitting a line to the relation.
2. The relation between stage and width reasonably represents a consistent measurement location that can be assumed to be representative of a reach average. Data that were clearly collected at a different location in the river as evidenced by a defined stage-width relation that exhibited obvious discontinuity on either the stage, width, or both axes of a width versus stage graphical plot (Fig. 2) were removed.
3. Data points that represent an overbank flow condition as evidenced by a clear discontinuity or distinct inflection point in the graphical plot of width versus stage (Fig. 2), or are above-referenced flood stage was removed. No additional verification of overbank was conducted under the assumption that no clear discontinuity would necessarily imply that the flow remains in a contiguous and confined channel rather than spreading out beyond the channel confines.

4) Individual measures of stage, width, or both that were not screened by criteria 2 or 3 above that nevertheless plotted well above or below (by $> \sim 20\%$) the general relation between width and stage and violated the monotonic and/or positive correlation *c* requirement (Fig. 2) were removed.

The quality control measures described above resulted in the removal of 13% of the measurements. The quality-controlled data set is publicly available through a USGS data release at Ref. 62.

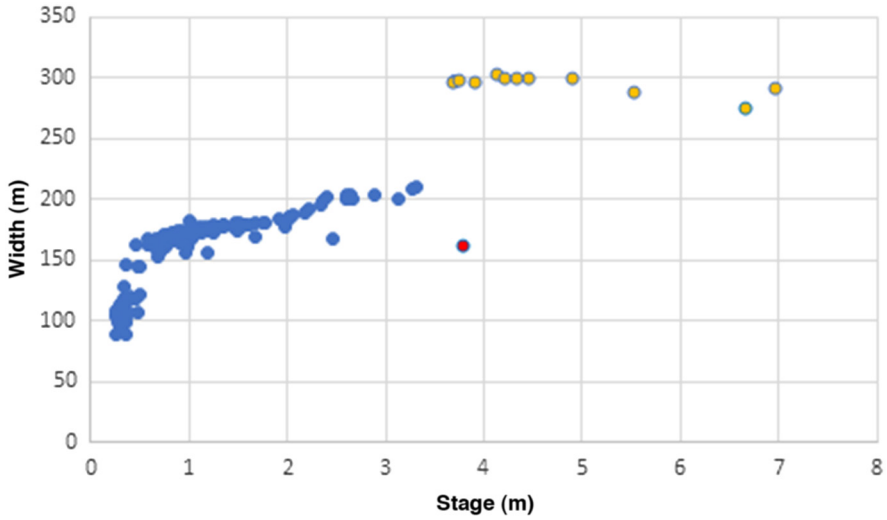

Fig. 2 Example of stage-width relation for the Susquehanna River near Waverley NY (station 01515000) with anomalous value outside of general trend (red point) that was removed from the data set, and values that represent overbank flow and/or measurement at a different cross-section (yellow points) were also removed from the data set.

2.1.3 *Algorithm calibration procedure*

The algorithm calibration proceeded by deriving a linear relation between width and stage assuming that the width varies with depth by a power function (e.g., parabolically—where the width squared varies linearly with stage). Using this relation, width was computed as a function of stage for each river. This step assures a uniform, monotonic linear increase in width with an increase in stage and assumes the calibrated width is representative of the average channel width for the reach. Figure 3 graphically displays the calibration process.

The maximum width in the derived time series and the maximum stage in the time series were assumed to represent bankfull channel dimensions. Bankfull values served as the reference point for determining relative depth in the channel. The bankfull depth in the channel for any given site was calculated from the following parabolic relation (bankfull stage – B)/1.5 where B (elevation of zero flow) is the no flow or bottom boundary of the assumed cross-section. The value 1.5 is the ratio of the maximum to mean depth in a cross-section that has a parabolic shape, with stage

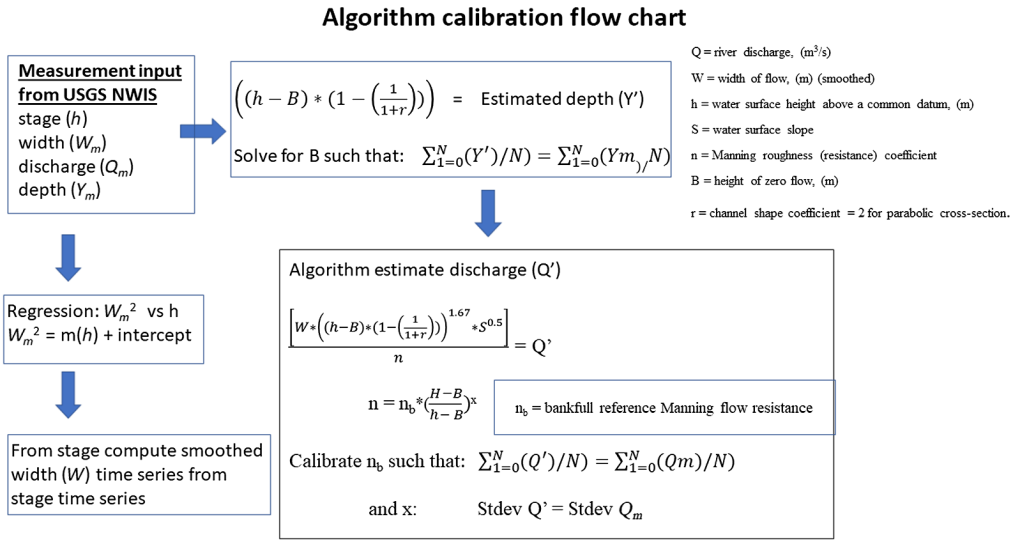

Fig. 3 Flow chart illustrating the procedure for calibrating the algorithm parameters – USGS National Water Information System (NWIS).

representing the change in depth at the center (deepest) part of the parabolic cross-section. The value of B was determined by matching the mean of the observed depths in the calibration data with the mean of the estimated depths determined from the observed stage minus B divided by 1.5 (see Fig. 3).

Calibration to all observed discharges proceeded by matching the mean and standard deviation of algorithm-estimated discharges to USGS observed discharges by adjusting the bankfull reference Manning n (fitted parameter n_b) and the exponent x of the Manning n transform function that relates the n_b to the relative depth as in Eq. (4). The parameter B was held constant.

An alternative calibration minimizes the normalized root mean square error (NRMSE; normalized to the mean flow) and maximizes the Kling–Gupta efficiency (KGE).[70,71] Comparing the two calibration methods shows very little difference, indicating that the algorithm optimizes to similar values using different calibration objectives.

2.1.4 *Algorithm performance and uncertainty—discharge calibration results*

The overall calibration results for the 30 rivers are provided in Table 2. In general, with the exception of the Tennessee River and the Pee Dee River, overall performance was good across the rivers—with mean values of NRMSE, log residual and percent residual within 10%, and Nash–Sutcliffe Efficiency (NSE[72]) and KGE averaging better than 0.94. Comparatively, the Tennessee River flow depth and slope are highly regulated by dams and for navigation. As such its flow regime does not necessarily conform to a flow resistance law primarily driven by gravity. Similarly, relative to other rivers the Pee Dee River discharge, flow depth, and slope are highly controlled and show a wide range due to dam operation.

2.1.5 *Calibration performance as a function of number of calibration points*

In practice, it is assumed there would be a limited number of observed *in-situ* discharges available for calibration. A Monte Carlo style experiment was conducted to determine an optimally minimum number of observations (calibration points) needed to reliably calibrate n_b and x in Eq. (4). Random, unique, and independent subsamples were taken from the USGS measurement data set for each river producing 100 sets of calibration results for a range of subsample sizes. The subsample sizes represented a different number of observations available for calibration, starting with two observations up to 40 observations. The calibration points for each subsample were compared to the calibration results using the entire record used for the complete calibration described above. The results using the entire record represent the objective values, which are considered to be the best possible estimate. As such, the full calibration is assumed to represent algorithm uncertainty apart from uncertainty associated with the input data and uncertainty associated with differences in river flow regime and morphology.

For example, the results for Willamette River show that the parameter values will converge to within 10% of the optimal n_b on average using seven randomly selected observations of discharge and within 10% of the optimum value for the parameter x on average using 20 calibration points (Fig. 4; Table 3). Additionally, the optimum value for the KGE converges using three calibration points on average (Table 3). Based on average values from these experiments, it may be concluded that a satisfactory calibration may be achieved by calibrating with a minimum of approximately six *in-situ* discharge observations (as measured by the KGE), and optimum values for the algorithm parameters will be attained when 13 to 19 calibration points are available.

These tests also indicate that the calibrated parameters stabilize even over several years of discharge observations used as calibration points, showing that the calibration and the parameters are not subject to substantial fluctuations over time.

2.1.6 *Error distribution and algorithm improvements*

Errors in the discharge estimates generated from the Manning algorithm applied in this study exhibit a pronounced positive bias for lower discharges in approximately one-third of the rivers

Table 2 Algorithm performance and uncertainty: comparative two-parameter calibration results.

		Calibrated best 2 parameter fit							
Station number	River name	Calibrated n_b	Calibrated x	NRMSE	NSE	Mean logRes (pct)	Mean PctRes	KGE	Occurrence of large low end bias (>20% log residual skewed to overestimation)
01184000	Connecticut River at Thompsonville, CT	0.023	4.1	0.19	0.96	−0.1	0.16	0.96	Yes
01434000	Delaware River at Port Jervis, NY	0.017	1.1	0.27	0.98	−0.14	0.17	0.96	Yes
01515000	Susquehanna River Near Waverly, NY	0.021	0.5	0.14	0.98	−0.17	0.26	0.97	Yes
01576000	Susquehanna River at Marietta, PA	0.037	1.4	0.11	0.99	−0.29	0.47	0.98	Yes
01638500	Potomac River at Point of Rocks, MD	0.021	0.4	0.31	0.97	−0.23	0.53	0.95	Yes
02087500	Neuse River near Clayton, NC	0.022	0.7	0.23	0.97	−0.13	0.15	0.96	Yes
02129000	Pee Dee R NR Rockingham, NC	0.015	3.1	0.33	0.93	−0.48	1.55	0.93	Yes
03593500	Tennessee River at Savannah, TN	0.023	8.3	0.36	0.38	−0.1	0.44	0.69	
05082500	Red River of the North at Grand Forks, ND	0.023	2.2	0.35	0.86	−0.23	0.45	0.91	Yes
06185500	Missouri River near Culbertson, MT	0.015	1.2	0.20	0.98	0.02	0	0.99	
6820500	Platte River near Agency, MO	0.03	0.5	0.34	0.96	−0.52	0.92	0.94	Yes
06934500	Missouri River at Hermann, MO	0.029	1	0.05	0.99	0	0	0.99	
7020500	Mississippi River at Chester, IL	0.024	0.8	0.04	0.99	0	0	1	
07022000	Mississippi River at Thebes, IL	0.023	0.5	0.08	0.98	0.02	−0.02	0.99	
9261000	Green River Near Jensen, UT	0.037	0.5	0.09	0.99	−0.04	0.05	0.99	
11377100	Sacramento R AB Bend Bridge NR Red Bluff, CA	0.031	−0.1	0.04	1.00	−0.01	0.01	0.99	

Table 2 (*Continued*).

Station number	River name	Calibrated best 2 parameter fit							
		Calibrated n_b	Calibrated x	NRMSE	NSE	Mean logRes (pct)	Mean PctRes	KGE	Occurrence of large low end bias (>20% log residual skewed to overestimation)
11389500	Sacramento R A Colusa, CA	0.038	0.2	0.07	0.99	−0.02	0.02	0.99	
12150800	Snohomish River Near Monroe, WA	0.012	1.9	0.24	0.94	−0.2	0.28	0.95	Yes
12399500	Columbia River at International Boundary	0.019	0.5	0.04	0.99	0.02	-0.02	0.99	
12422500	Spokane River at Spokane, WA	0.043	2.4	0.10	0.99	−0.16	0.26	0.98	Yes
12462500	Wenatchee River at Monitor, WA	0.029	1	0.12	0.99	−0.1	0.13	0.98	Yes
14191000	Willamette River at Salem, OR	0.022	0.5	0.10	0.99	−0.04	0.05	0.99	
15304000	Kuskokwim R at Crooked Creek, AK	0.018	0.9	0.07	0.97	−0.03	0.04	0.99	
15356000	Yukon R at Eagle, AK	0.022	0.4	0.06	0.97	−0.01	0.04	0.98	
15453500	Yukon R NR Stevens Village, AK	0.023	0.5	0.04	0.99	0.02	−0.02	0.99	
15485500	Tanana R at Fairbanks, AK	0.037	−0.3	0.14	0.92	0.06	−0.02	0.96	
15515500	Tanana R at Nenana, AK	0.034	1.3	0.07	0.98	0	0.01	0.99	
15565447	Yukon R at Pilot Station, AK	0.019	2.5	0.13	0.83	−0.01	0.03	0.92	
15875000	Colville R at Umiat, AK	0.028	1.5	0.13	0.99	−0.06	0.64	0.99	
15908000	Sagavanirktok R NR Pump STA 3, AK	0.031	1.7	0.26	0.86	−0.04	0.08	0.93	

Table 2 (*Continued*).

Station number	River name	Calibrated best 2 parameter fit							
		Calibrated n_b	Calibrated x	NRMSE	NSE	Mean logRes (pct)	Mean PctRes	KGE	Occurrence of large low end bias (>20% log residual skewed to overestimation)
	Mean	0.026	1.4	0.16	0.94	−0.10	0.22	0.96	
	Stdev	0.008	1.6	0.11	0.12	0.14	0.34	0.06	
	Max	0.043	8.3	0.36	1.00	0.06	1.55	1.00	
	Min	0.012	−0.3	0.04	0.38	−0.52	−0.02	0.69	
	Median	0.023	1.0	0.13	0.98	−0.04	0.07	0.98	
	75th	0.031	1.7	0.24	0.99	0.00	0.28	0.99	
	25th	0.021	0.5	0.07	0.96	−0.16	0.01	0.95	
	Alaskan Rivers								
	Mean	0.027	1.1	0.11	0.94	−0.01	0.10	0.97	
	stdev	0.007	0.9	0.07	0.06	0.04	0.22	0.03	
	max	0.037	2.5	0.26	0.99	0.06	0.64	0.99	
	min	0.018	−0.3	0.04	0.83	−0.06	−0.02	0.92	
	Median	0.026	1.1	0.10	0.97	−0.01	0.04	0.99	
	75th	0.032	1.6	0.13	0.98	0.01	0.05	0.99	
	25th	0.021	0.5	0.07	0.91	−0.03	0.00	0.95	

n_b, bankfull reference Manning n; x, exponent of Manning n function; EZF, elevation of zero flow in channel (channel bottom); NRMSE, normalized root mean square error; NSE, Nash–Sutcliffe efficiency statistic; logRes, the log of the RSQ estimate minus the log of the observed discharge; PctRes, RSQ estimated discharge minus the observed discharge divided by the observed discharge; KGE, Kling–Gupta efficiency; RSQ, remote sensing discharge.

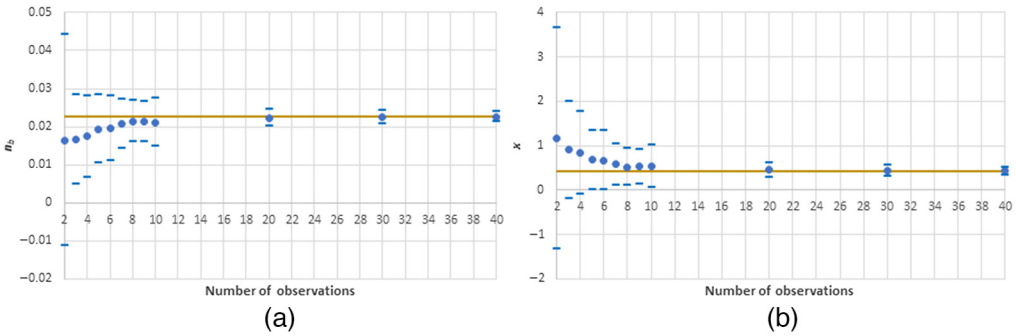

Fig. 4 Example Monte Carlo experiment n_b and x calibration results for the Willamette River at Salem (station 14191000) showing the mean Manning reference flow resistance (n_b) (a) and the exponent of the Manning n function (x) (b) in the subsampled groups (points) and two standard deviations above and below the mean (bars) compared to the control n_b and x values calibrated from the entire record (horizontal line). As the number of calibration points increases, the mean values converge toward the control value and standard deviation decreases.

(examples shown in Fig. 5). Note that the mean bias was near zero for the calibrated models because the calibration included matching the mean (Table 2).

The low-end bias indicates that the Manning n is underestimated at low flows relative to the middle and upper end of the hydrograph. This is likely because the hydraulic flow resistance at low flow becomes more influenced by individual flow obstructions on the bed and banks in the river.[73] Flow may become less turbulent in some portions of the reach and more turbulent in others because flow paths may diverge and become directed vertically and laterally, wave resistance becomes more significant as depth becomes shallower, and greater portions of the cross-section may not contribute to downstream conveyance (i.e., dead zones develop in the flow cross-section).

The largest error (and greatest uncertainty) in the discharge estimates occur at low flow for rivers that show the low-end bias (Fig. 5; Table 2; examples include the Pee Dee River, the Neuse River, the Potomac River). These rivers tend to be those with very low slopes and a wide range of discharge, and/or the flow regime at lower flow is dominated by obstructions. This same trend, although not nearly as prominent, is evident for many rivers that do not show the bias, indicating that the assumption of a linear function for transforming Manning n flow resistance breaks down at low discharge as the relation between depth and flow resistance becomes non-linear. Examining the aggregate record of estimated discharge for all of the test rivers shows that the error (uncertainty) is clearly also related to the depth of flow and the discharge.

Three of the study rivers exhibit high errors, the Tennessee River, the Pee Dee River, and the Red River. The Tennessee River error is seen across the entire range of flow and not concentrated at the low end. This is attributed to flow, depth, and slope control by several dams along the channel both upstream and downstream of the measurement reach. The Pee Dee River shows the highest percent errors of any river, especially at the low end of the discharge and depth range of flow. The Pee Dee also has dams along the river reach that control the flow, depth, and slope, and exhibits very low Froude numbers at the low end of the discharge range. The Froude (F) number represents the ratio of inertial to gravitational forces in the flow,[48,51] and is computed directly from the USGS flow measurement data as the ratio of the mean velocity divided by the square root of the gravitation acceleration constant times the mean depth ($F = \sqrt{\frac{V}{gY}}$, where V is the mean velocity, Y is the mean depth, and g is the gravitational acceleration constant).

The low Froude numbers may indicate that significant portions of the cross-section are not contributing to downstream flow due to stagnant water or pooling of water, with section control dominating the flow regime. The flow regime of both of these rivers reaches is considered to violate the assumptions inherent in the discharge algorithm that the channel control is the dominant control on slope, depth, velocity, and discharge. The Red River shows a majority of discharge estimates exhibiting relatively high error also at the low end of the discharge range with very low Froude numbers similar to the Pee Dee River. The Red River calibration is skewed to

Table 3 Calibration performance as a function of number of calibration points: convergence characteristics for the two-parameter calibration results.

Station Number	River name	Number of calibration points to converge on stable value for n_b	Number of calibration points to converge on stable value for x	Number of calibration points to converge on stable value for KGE
01184000	Connecticut River at Thompsonville, CT.	20	20	4
01434000	Delaware River at Port Jervis, NY	40	40	7
01515000	Susquehanna River near Waverly, NY	20	40	3
01576000	Susquehanna River at Marietta, PA	8	20	4
01638500	Potomac River at Point of Rocks, MD	40	40	8
02087500	Neuse River near Clayton, NC	20	30	8
02129000	Pee Dee R NR Rockingham, NC	40	40	8
03593500	Tennessee River at Savannah, TN	5	4	4
05082500	Red River of the North at Grand Forks, ND	20	30	7
06185500	Missouri River near Culbertson, MT	30	30	30
6820500	Platte River near Agency, MO	40	40	7
06934500	Missouri River at Hermann, MO	3	3	4
7020500	Mississippi River at Chester, IL	3	3	6
07022000	Mississippi River at Thebes, IL	3	3	5
9261000	Green River near Jensen, UT	5	30	4
11377100	Sacramento R AB Bend Bridge NR Red Bluff, CA	3	4	4
11389500	Sacramento R A Colusa, CA	6	20	5
12150800	Snohomish River near Monroe, WA	30	30	3
12399500	Columbia River at International Boundary	4	3	3
12422500	Spokane River at Spokane, WA	6	7	3
12462500	Wenatchee River at Monitor, WA	9	20	4
14191000	Willamette River at Salem, OR	7	20	3
15304000	Kuskokwim R at Crooked Creek, AK	3	20	7
15356000	Yukon R at Eagle, AK	3	8	4
15453500	Yukon R NR Stevens Village, AK	3	6	3
15485500	Tanana R at Fairbanks, AK	10	20	6
15515500	Tanana R at Nenana, AK	3	7	6
15565447	Yukon R at Pilot Station, AK	4	7	6
15875000	COLVILLE R AT UMIAT AK	5	4	10
15908000	Sagavanirktok R NR Pump STA 3, AK	3	20	4

Table 3 (*Continued*).

Station Number	River name	Number of calibration points to converge on stable value for n_b	Number of calibration points to converge on stable value for x	Number of calibration points to converge on stable value for KGE
	Mean	13	19	6
	Stdev	13	13	5
	Max	40	40	30
	Min	3	3	3
	Median	6	20	5
	75th	20	30	7
	25th	3	6	4
	Alaskan rivers			
	Mean	4	12	6
	Stdev	2	7	2
	Max	10	20	10
	Min	3	4	3
	Median	3	8	6
	75th	4	20	6
	25th	3	7	4

n_b, bankfull reference Manning n value; x, exponent on the relative depth Manning n function; number of calibration points to converge, the number of measurements needed to calibrate to a relatively stable value equal to the value of all observations points are used to calibrate; KGE, Kling–Gupta efficiency.

the low end because there are fewer midrange and high flow measurements that deviate from the stage-discharge trend defined by the lower discharges. This indicates that there are several flow regimes that are not adequately represented by a single flow resistance function. For this reason, the Red River also violates the general assumptions of the discharge algorithm. As such, these data were removed from the discharge database to facilitate further examination of the error trends among the remaining sites.

The percent fractional error for all of the estimated discharges in the discharge data set (excluding the Tennessee, Pee Dee, and Red River data) is largest at depths below 3 m [Fig. 6(a)], and discharge below $\sim$1000 m^3/s [Fig. 6(b)]. The relation between error and discharge shows a distinct trend line [Fig. 6(b)] with decreasing error with discharge, although the trend line does not show a strong coefficient of determination (R^2).

We tested a calibration procedure that allowed the parameter B to be a freely adjusted parameter instead of assuming this to be a measured value. While this three-parameter calibration (n_b, x, and B) increased the number of degrees of freedom, the calibration was able to reduce low-end bias in many rivers. However, it was found that in almost all cases (with the exception of the Tanana River at Fairbanks, the Platte River, and the Columbia River) the calibrated value of B was higher than observed resulting in shallower estimated depths, higher estimated velocities, and larger Froude numbers compared to the observed values with only marginal improvement in overall predictive power compared to using a measured depth.

The low-end bias has been observed in a general way when applying a Manning type equation to flows in many rivers,[25,74] which is hypothesized here to be due to a non-linear relationship between flow depth and flow resistance, although nonlinearity between flow resistance and slope

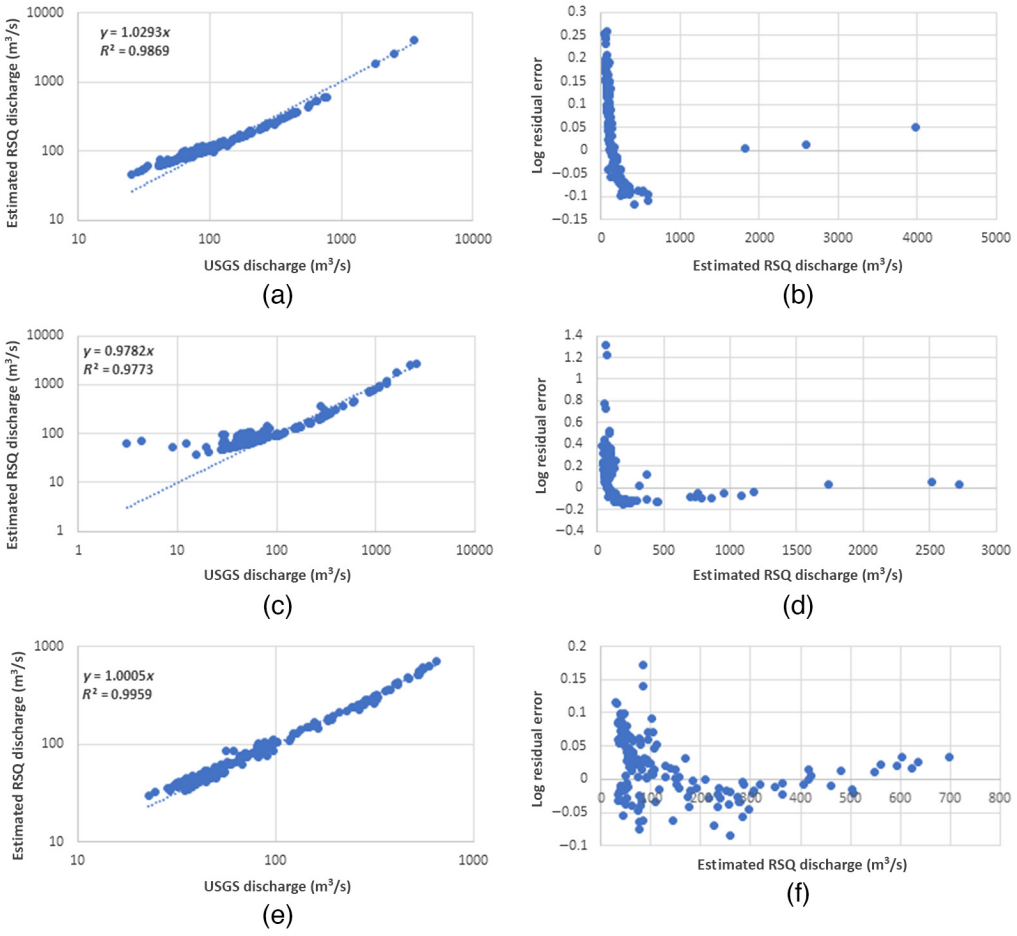

Fig. 5 Comparative RSQ estimate versus USGS ground-based gaged discharge (left panel) and error distribution as a function of the RSQ estimate (right panel) for three example rivers. (a) and (b) the Delaware, (c) and (d) Potomac, and (e) and (f) Green.

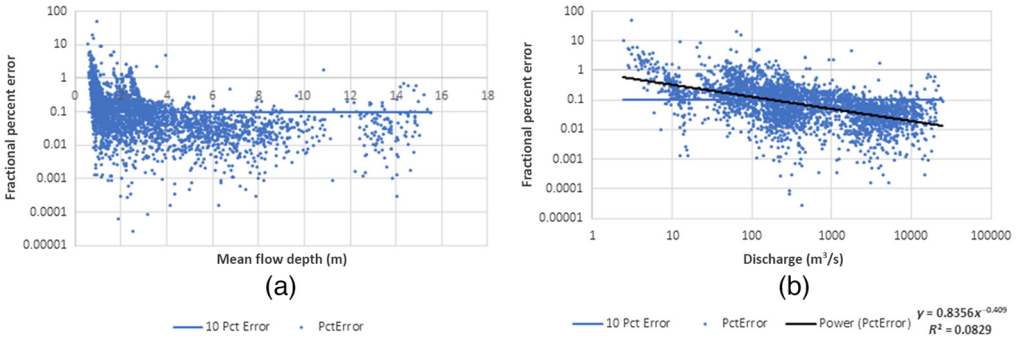

Fig. 6 (a) and (b) Absolute value of percent error of discharge for the aggregate estimated discharges for the 30 study rivers plotted against the estimated depth of flow and for each discharge—note that this plot excludes the Tennessee, Pee Dee, and Red Rivers, as the depths of these rivers are considered to be artificially controlled or the flow does not meet assumptions of channel control due to excessive stagnant water in the channel. (b) The linear trend between discharge and error.

and width may also be important. Dingman and Sharma[74] adjusted their statistically derived Manning type equation for non-linearity in slope. The roughness height/boundary layer theory[48] can be incorporated into the Manning n transformation function by adding an additive term that includes a roughness height layer that does not effectively contribute to the uniform flow field.

This results in a function that progressively offers more resistance to flow as the depth becomes shallower because the roughness height becomes more dominant relative to the full depth of flow. However, this approach can result in negative discharges when the roughness height exceeds the minimum height in the stage observations.

We adjusted for this observed nonlinearity by assuming the exponent x varies with relative depth to derive Eq. (5) recognizing the formulation presented in Eq. (4) results in over estimation of the low discharge. Therefore, a factor that would reduce the value of x with relative depth would have the result of increasing flow resistance and decreasing discharge as depth decreases. We also used relative depth in the nonlinear function because it can be readily measured from satellites by tracking WSF. Future improvements may also include relative change in slope and width as nonlinear parameters. As such, we adopt Eq. (5) as the most robust Manning n transform and adapt the overall strategy to measure depth (B) rather than let it be a freely calibrated parameter

$$n = n_b * \left(\frac{H-B}{h-B}\right) \exp\left(x * \left(\frac{H-B}{h-B}\right)\right). \tag{5}$$

Figures 7–9 show the results of the initial two-parameter calibration, the three-parameter calibration, and the modified Manning transformation function calibration for selected rivers. Comparative results for the three calibrations are shown in Table 4.

The three-parameter calibration (optimized values for the value of B, n_b, and x) eliminated low-end bias and reduced error as compared to the initial two parameter calibration (Fig. 7), which used the observed depth to define the value of B (Fig. 9). However, to achieve the reduction in bias, the Froude number, as an index to hydraulic state of flow, is much larger due to shallower depth (increasing value of B) and predicted higher velocity. Thus, the three-parameter calibration improved on the low-end bias at the expense of realism in the hydraulics. Note also that the largest error is still concentrated at the low end of the discharge.

The calibration results for Eq. (5) (Fig. 8) are similar to the three-parameter calibration, successfully eliminating the low-end bias and reducing overall error with the advantage that it does not introduce an additional parameter that requires calibration, enabling the value of B to remain a measurable parameter.

The results of the three calibration options show that the two-parameter calibration with the modified (and nonlinear) Manning n transform function (where n_b and x are calibrated holding B constant) performs as well overall compared to the three-parameter calibration (Table 4). Increasing error is associated with a wider range of predicted Froude numbers (meaning wider range of flow conditions) as indexed by the ratio of the maximum to minimum Froude number (Fig. 10). This indicates that the preferred algorithm option for rivers with an expected wider range of flow would be the nonlinear Manning n transform [Eq. (5)].

The overall NRMSE is also correlated with normalized stream power (Table 1) as defined and provided by Frasson et al.[19] and illustrated in Fig. 11 (Stream power is defined in Frasson et al.,[19] as the weight density of water times the flow rate times the slope, Power $= Q\gamma S$). Rivers with stream power <200 W/m are the rivers with the highest NRMSE. Froude number and stream power are strong indicators of algorithm performance.

Examining the aggregate error for all of the flows from the 30 rivers (Fig. 6) excluding the Tennessee and Pee Dee Rivers (due to flow controls by dams), as well as the Red and Pee Dee Rivers due to very low streampower (e.g., flow is more like flow through pools rather than flow controlled by slope with very low Froude numbers), we summarized threshold stats for NRMSE associated with depth and discharge (Table 5). Considering a depth threshold of >2 m the data show that 52% have an error of 5% or less and 74% have an error of 10% or less compared to 39% and 58% for all flows. Using a threshold of >3 m, 63% are below 5% error and 87% below 10% error. Considering a discharge threshold of >1000 m^3/s, the data show that 65% have an error of 5% or less and 88% have an error of 10% or less compared to 39% and 58% for all flows. Using a threshold of >2000 m^3/s, 71% are below 5% error and 92% below 10% error.

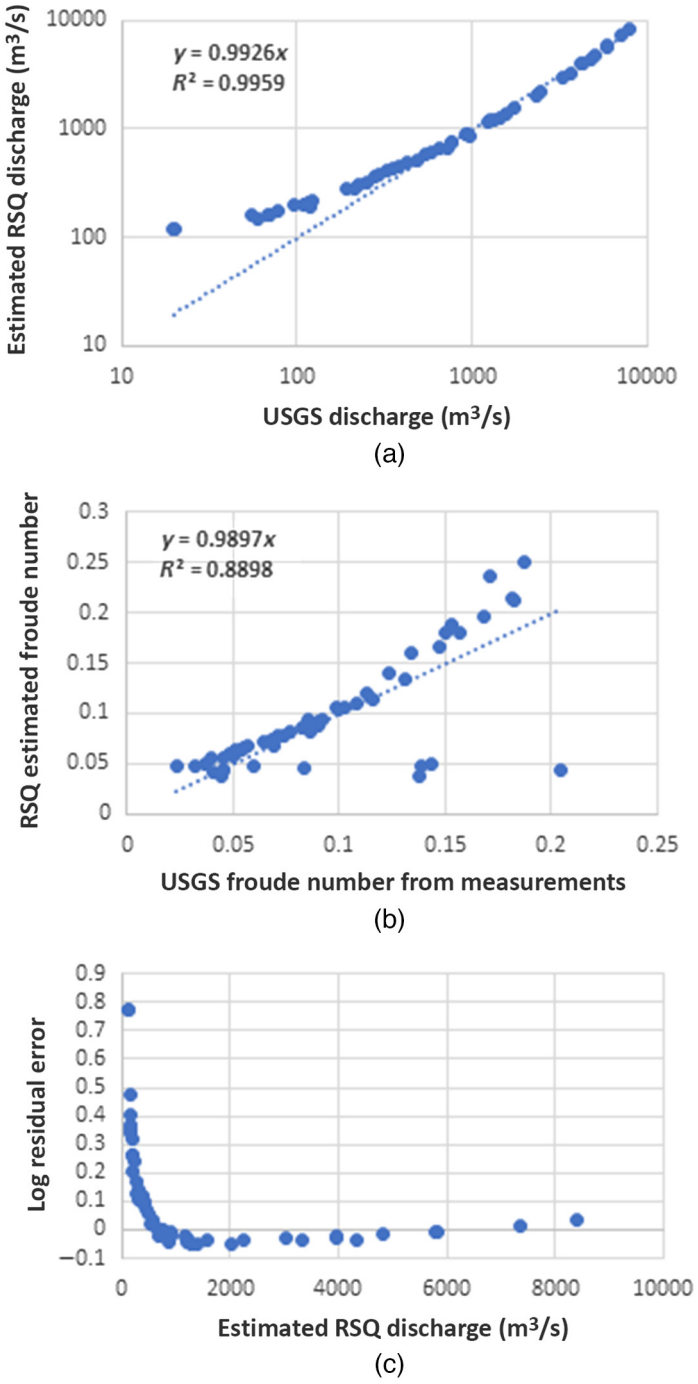

Fig. 7 Calibrated discharge estimates for the two-parameter (initial) calibration showing (a) the predicted discharge versus the observed discharge, (b) the predicted Froude number versus the observed Froude number, and (c) the error versus predicted discharge for the Susquehanna River at Marietta (station 01576000). USGS, U.S. Geological Survey; RSQ, remote sensing discharge.

2.2 *Remote Sensing Observations Data Uncertainty*

The remotely sensed river observations consist of the WSE, the width of the water-surface, and the water-surface slope. Although we anticipate limited ground-based observations of the discharge, velocity, and reach bathymetry to calibrate the RSQ estimates, we do not consider ground-based measurement error in this section, and it is generally assumed that uncertainty associated with ground-based observations is negligible. Validation studies for both observed

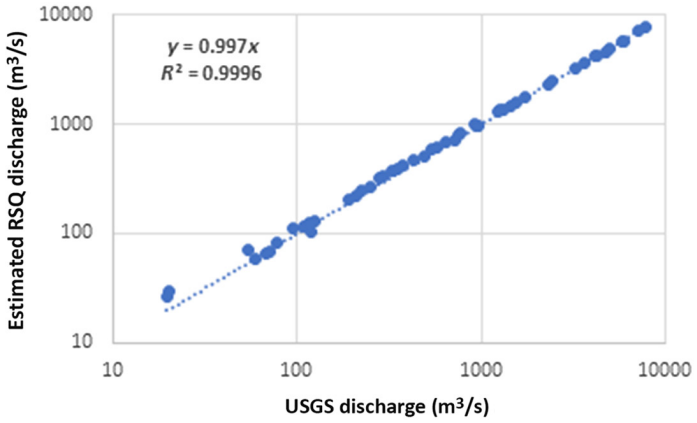

(a)

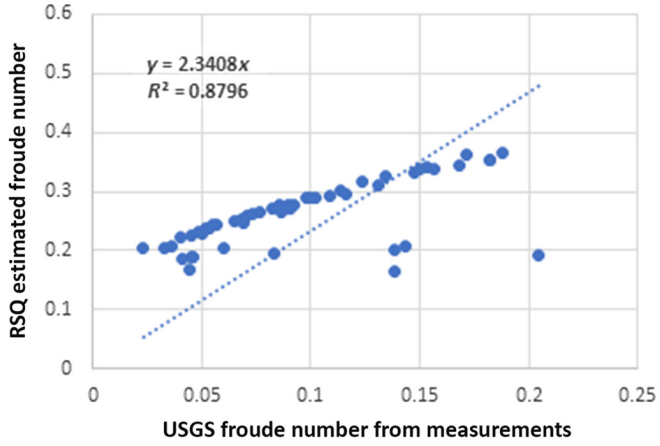

(b)

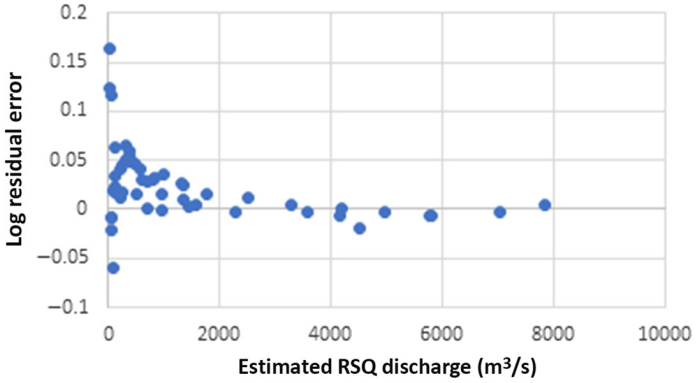

(c)

Fig. 8 Calibrated discharge estimates for the three-parameter (initial) calibration showing (a) the predicted discharge versus the observed discharge, (b) the predicted Froude number versus the observed Froude number, and (c) the error versus predicted discharge (C) for the Susquehanna River at Marietta (station 01576000). USGS, U.S. Geological Survey; RSQ, remote sensing discharge.

variables have been conducted at many locations using different instruments mounted on various satellite platforms providing first-order expected observation accuracies. Along with these studies, the spatial (x, y, and z) accuracies are generally reported based on the specifications of the observing instruments, including discussion of factors that may reduce accuracy.

Recently, observations of water-surface height in rivers (and other water bodies) derived from the Jason-2 and Jason-3 satellite nadir altimeter missions provide an estimate of

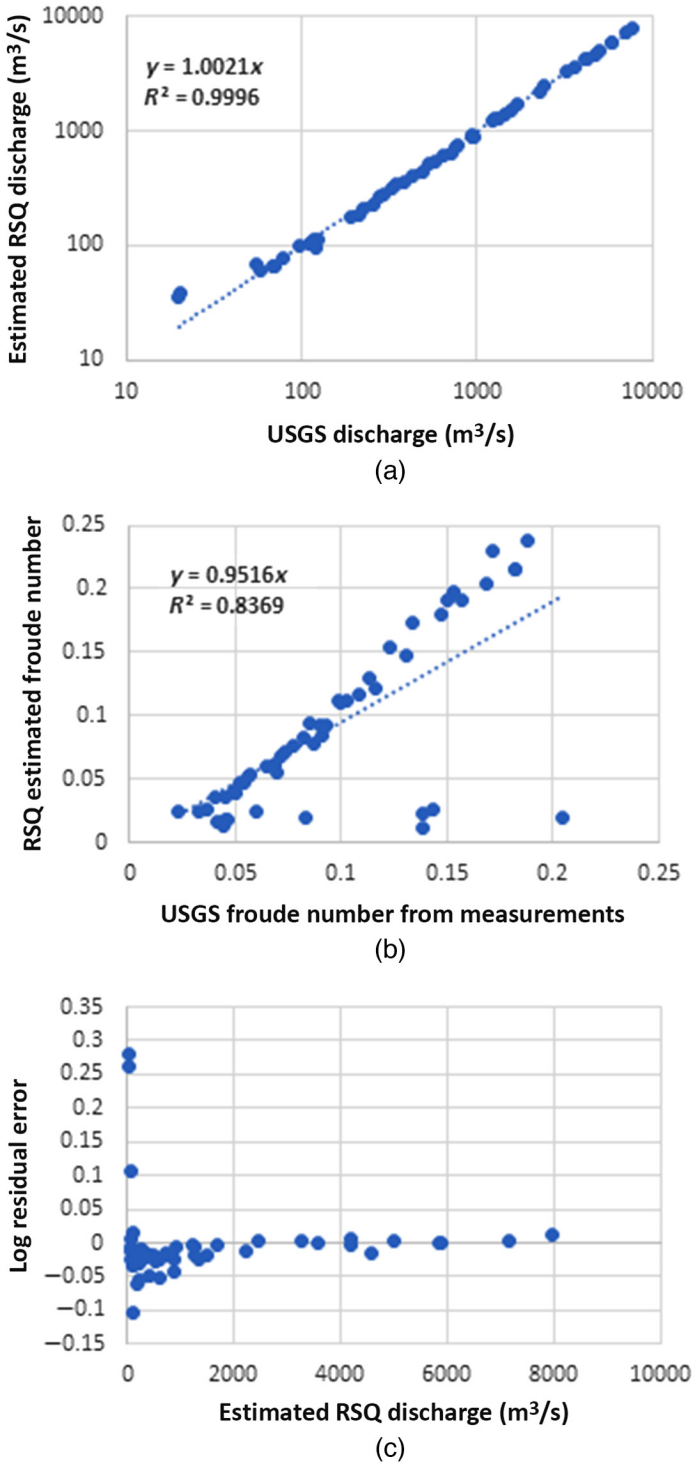

Fig. 9 Calibrated discharge estimates for the two-parameter calibration with the modified Manning *n* transform [Eq. (5)] showing (a) the predicted discharge versus the observed discharge, (b) the predicted Froude number versus the observed Froude number, and (c) the error versus predicted discharge for the Susquehanna River at Marietta (station 01576000). USGS, U.S. Geological Survey; RSQ, remote sensing discharge.

observational error. These estimates are based on qualitative characteristics of the target as well as atmospheric and instrument conditions and responses. As such, they are not precise errors but rather provide an expected error based on qualitative characteristics of the observation.[43]

Table 4 Comparative calibration results for two- and three-parameter calibration of RSQ.

Station number	River name	Calibrated n_b	Calibrated x	Calibrated B	NRMSE	NSE	Mean logRes (PCT)	Mean PctRes
			Calibrated best 2 parameter fit					
01184000	Connecticut River at Thompsonville, CT	0.023	4.1	−1.9	0.19	0.96	−0.1	0.16
01434000	Delaware River at Port Jervis, NY	0.017	1.1	−0.7	0.27	0.98	−0.14	0.17
01515000	Susquehanna River Near Waverly, NY	0.021	0.5	−0.9	0.14	0.98	−0.17	0.26
01576000	Susquehanna River at Marietta, PA	0.037	1.4	7.1	0.11	0.99	−0.29	0.47
01638500	Potomac River at Point of Rocks, MD	0.021	0.4	−0.8	0.31	0.97	−0.23	0.53
02087500	Neuse River Near Clayton, NC	0.022	0.7	−0.7	0.23	0.97	−0.13	0.15
02129000	Pee Dee R NR Rockingham, NC	0.015	3.1	−3.5	0.33	0.93	−0.48	1.55
03593500	Tennessee River at Savannah, TN	0.023	8.3	−9.8	0.36	0.38	−0.1	0.44
05082500	Red River of the North at Grand Forks, ND	0.023	2.2	−0.6	0.35	0.86	−0.23	0.45
06185500	Missouri River near Culbertson, MT	0.015	1.2	−1.9	0.20	0.98	0.02	0
6820500	Platte River near Agency, MO	0.03	0.5	0.5	0.34	0.96	−0.52	0.92
06934500	Missouri River at Hermann, MO	0.029	1	−5.5	0.05	0.99	0	0
7020500	Mississippi River at Chester, IL	0.024	0.8	−7.8	0.04	0.99	0	0
07022000	Mississippi River at Thebes, IL	0.023	0.5	−6.3	0.08	0.98	0.02	−0.02
9261000	Green River near Jensen, UT	0.037	0.5	−0.5	0.09	0.99	−0.04	0.05
11377100	Sacramento R AB Bend Bridge NR Red Bluff, CA	0.031	−0.1	−1.5	0.04	1.00	−0.01	0.01
11389500	Sacramento R A Colusa, CA	0.038	0.2	8	0.07	0.99	−0.02	0.02
12150800	Snohomish River near Monroe, WA	0.012	1.9	−3.3	0.24	0.94	−0.2	0.28
12399500	Columbia River at International Boundary	0.019	0.5	22.6	0.04	0.99	0.02	−0.02
12422500	Spokane River at Spokane, WA	0.043	2.4	2.2	0.10	0.99	−0.16	0.26
12462500	Wenatchee River at Monitor, WA	0.029	1	3.9	0.12	0.99	−0.1	0.13
14191000	Willamette River at Salem, OR	0.022	0.5	−1.5	0.10	0.99	−0.04	0.05

Table 4 (*Continued*).

Station number	River name	Calibrated n_b	Calibrated x	Calibrated B	NRMSE	NSE	Mean logRes (PCT)	Mean PctRes
15304000	Kuskokwim R at Crooked Creek, AK	0.018	0.9	−4.7	0.07	0.97	−0.03	0.04
15356000	Yukon R at Eagle, AK	0.022	0.4	−3.5	0.06	0.97	−0.01	0.04
15453500	Yukon R NR Stevens Village, AK	0.023	0.5	−0.9	0.04	0.99	0.02	−0.02
15485500	Tanana R at Fairbanks, AK	0.037	-0.3	2.1	0.14	0.92	0.06	−0.02
15515500	Tanana R at Nenana, AK	0.034	1.3	−4.4	0.07	0.98	0	0.01
15565447	Yukon R at Pilot Station, AK	0.019	2.5	−14.2	0.13	0.83	−0.01	0.03
15875000	Colville R at Umiat, AK	0.028	1.5	11.4	0.13	0.99	−0.06	0.64
15908000	Sagavanirktok R NR Pump STA 3, AK	0.031	1.7	3.3	0.26	0.86	−0.04	0.08
	Mean	0.026	1.4	−0.5	0.16	0.94	−0.10	0.22
	Stdev	0.008	1.6	6.7	0.11	0.12	0.14	0.34
	Max	0.043	8.3	22.6	0.36	1.00	0.06	1.55
	Min	0.012	−0.3	−14.2	0.04	0.38	−0.52	−0.02
	Median	0.023	1.0	−0.9	0.13	0.98	−0.04	0.07
	75th	0.031	1.7	1.7	0.24	0.99	0.00	0.28
	25th	0.021	0.5	−3.5	0.07	0.96	−0.16	0.01
	Alaskan rivers							
	Mean	0.027	1.1	−1.4	0.11	0.94	−0.01	0.10
	stdev	0.007	0.9	7.4	0.07	0.06	0.04	0.22
	Max	0.037	2.5	11.4	0.26	0.99	0.06	0.64
	Min	0.018	−0.3	−14.2	0.04	0.83	−0.06	−0.02
	median	0.026	1.1	−2.2	0.10	0.97	−0.01	0.04
	75th	0.032	1.6	2.4	0.13	0.98	0.01	0.05
	25th	0.021	0.5	−4.5	0.07	0.91	−0.03	0.00

Table 4 (*Continued*).

Station number	River name	Calibrated n_b	Calibrated x	Calibrated B	NRMSE	NSE	Mean logRes (PCT)	Mean PctRes
		Calibrated best two parameter fit using modified Manning *n* function						
01184000	Connecticut River at Thompsonville, CT	0.024	2.9	−1.9	0.12	0.98	−0.1	0.14
01434000	Delaware River at Port Jervis, NY	0.02	0.3	−0.7	0.09	1	0	0.01
01515000	Susquehanna River near Waverly, NY	0.022	0.2	−0.9	0.1	0.99	−0.1	0.13
01576000	Susquehanna River at Marietta, PA	0.039	0.7	7.1	0.03	1	0.01	0
01638500	Potomac River at Point of Rocks, MD	0.021	0.1	−0.8	0.25	0.98	−0.18	0.42
02087500	Neuse River near Clayton, NC	0.022	0.3	−0.7	0.21	0.97	−0.03	0.04
02129000	Pee Dee R NR Rockingham, NC	0.016	1.8	−3.5	0.22	0.97	−0.36	0.84
03593500	Tennessee River at Savannah, TN	0.024	7.2	−9.8	0.35	0.4	−0.07	0.41
05082500	Red River of the North at Grand Forks, ND	0.025	1.3	−0.6	0.3	0.9	−0.2	0.38
06185500	Missouri River near Culbertson, MT	0.015	0.6	−1.9	0.26	0.98	0.08	−0.04
6820500	Platte River near Agency, MO	0.035	0.1	0.5	0.29	0.97	−0.46	0.73
06934500	Missouri River at Hermann, MO	0.03	0.6	−5.5	0.05	0.99	0	0.01
7020500	Mississippi River at Chester, IL	0.024	0.5	−7.8	0.05	0.99	0	0
07022000	Mississippi River at Thebes, IL	0.023	0.3	−6.3	0.08	0.98	0.02	−0.02
9261000	Green River near Jensen, UT	0.039	0.2	−0.5	0.07	1	0.01	−0.01
11377100	Sacramento R AB Bend Bridge NR Red Bluff, CA	0.029	0	−1.5	0.06	0.99	0.01	−0.01
11389500	Sacramento R A Colusa, CA	0.038	0.1	8	0.07	0.99	0.01	−0.01
12150800	Snohomish River near Monroe, WA	0.013	1	−3.3	0.16	0.97	−0.15	0.18
12399500	Columbia River at International Boundary	0.019	0.3	22.6	0.04	0.99	0.03	−0.02
12422500	Spokane River at Spokane, WA	0.045	1.5	2.2	0.05	1	−0.07	0.08
12462500	Wenatchee River at Monitor, WA	0.032	0.4	3.9	0.06	1	−0.05	0.06

Table 4 (*Continued*).

Station number	River name	Calibrated n_b	Calibrated x	Calibrated B	NRMSE	NSE	Mean logRes (PCT)	Mean PctRes
14191000	Willamette River at Salem, OR	0.023	0.2	−1.5	0.07	1	0	0
15304000	Kuskokwim R at Crooked Creek, AK	0.019	0.5	−4.7	0.07	0.98	−0.02	0.03
15356000	Yukon R at Eagle, AK	0.023	0.2	−3.5	0.06	0.97	0	0.03
15453500	Yukon R NR Stevens Village, AK	0.023	0.3	−0.9	0.02	1	0.01	−0.01
15485500	Tanana R at Fairbanks, AK	0.037	-0.3	2.1	0.14	0.92	0.02	0.02
15515500	Tanana R at Nenana, AK	0.035	0.9	−4.4	0.07	0.98	0.01	−0.01
15565447	Yukon R at Pilot Station, AK	0.0	2.5	−14.2	0.1	0.8	0.1	0.0
15875000	Colville R at Umiat, AK	0.03	0.8	11.4	0.16	0.98	0.22	−0.03
15908000	Sagavanirktok R NR Pump STA 3, AK	0.034	1	3.3	0.25	0.87	0.02	0.02
	Mean	0.027	0.9	−0.5	0.13	0.95	−0.04	0.11
	Stdev	0.008	1.4	6.7	0.09	0.11	0.13	0.22
	Max	0.045	7.2	22.6	0.35	1.00	0.22	0.84
	Min	0.013	-0.3	−14.2	0.02	0.40	−0.46	−0.04
	Median	0.024	0.5	−0.9	0.09	0.98	0.00	0.02
	75th	0.034	1.0	1.7	0.20	0.99	0.01	0.12
	25th	0.021	0.2	−3.5	0.06	0.97	−0.07	−0.01
	Alaskan rivers							
	Mean	0.028	0.7	−1.4	0.11	0.94	0.04	0.00
	Stdev	0.007	0.8	7.4	0.07	0.07	0.08	0.03
	Max	0.037	2.5	11.4	0.25	1.00	0.22	0.03
	Min	0.019	−0.3	−14.2	0.02	0.80	−0.02	−0.04
	Median	0.027	0.7	−2.2	0.11	0.98	0.02	0.01
	75th	0.034	0.9	2.4	0.15	0.98	0.03	0.02
	25th	0.022	0.3	−4.5	0.07	0.91	0.01	−0.02

Table 4 (*Continued*).

Station number	River name	Calibrated n_b	Calibrated x	Calibrated B	NRMSE	NSE	Mean logRes (PCT)	Mean PctRes
			Calibrated best 3 parameter fit					
01184000	Connecticut River at Thompsonville, CT	0.005	−0.4	2.2	0.15	0.97	0.12	−0.12
01434000	Delaware River at Port Jervis, NY	0.015	0.3		0.11	1	−0.01	0.02
01515000	Susquehanna River Near Waverly, NY	0.013	−0.3	0.1	0.12	0.99	0.02	−0.02
01576000	Susquehanna River at Marietta, PA	0.024	0.11	9.1	0.03	1	−0.06	0.06
01638500	Potomac River at Point of Rocks, MD	0.018	−0.4	0.0	0.17	0.99	−0.15	0.37
02087500	Neuse River near Clayton, NC	0.015	−0.4	0.2	0.16	0.98	0.06	−0.05
02129000	Pee Dee R NR Rockingham, NC	0.004	0.7	−0.1	0.79	0.62	0.04	−0.01
03593500	Tennessee River at Savannah, TN	0.001	1.3	1.5	0.61	−0.77	0.58	−0.23
05082500	Red River of the North at Grand Forks, ND	0.007	−0.8	−2.0	0.19	0.96	−0.07	0.09
06185500	Missouri River near Culbertson, MT	0.016	1.2	0.9	0.2	0.98	0.02	0
6820500	Platte River near Agency, MO	0.022	0.8	−2.0	0.63	0.86	0.33	−0.25
06934500	Missouri River at Hermann, MO	0.018	0	−3.4	0.05	0.99	−0.02	0.02
7020500	Mississippi River at Chester, IL	0.015	−0.2	−0.9	0.07	0.98	−0.06	0.06
07022000	Mississippi River at Thebes, IL	0.013	−0.7		0.11	0.96	−0.04	0.05
9261000	Green River Near Jensen, UT	0.032	0.3	−0.2	0.09	0.99	0.03	−0.03
11377100	Sacramento R AB Bend Bridge NR Red Bluff, CA	0.027	−0.4	−0.8	0.06	0.99	0.02	−0.02
11389500	Sacramento R A Colusa, CA	0.031	−0.3	9.9	0.08	0.99	0.02	−0.02
12150800	Snohomish River Near Monroe, WA	0.006	−0.1	−0.2	0.15	0.98	−0.03	0.03
12399500	Columbia River at International Boundary	0.022	0.9	20.9	0.04	0.99	0	0
12422500	Spokane River at Spokane, WA	0.019	0.5	4.5	0.09	0.99	0.04	−0.04
12462500	Wenatchee River at Monitor, WA	0.019	0	4.8	0.1	0.99	−0.02	0.03
14191000	Willamette River at Salem, OR	0.016	−0.4	0.6	0.05	1	−0.03	0.03
15304000	Kuskokwim R at Crooked Creek, AK	0.012	0	−2.0	0.08	0.97	0.04	−0.04

Table 4 (*Continued*).

Station number	River name	Calibrated n_b	Calibrated x	Calibrated B	NRMSE	NSE	Mean logRes (PCT)	Mean PctRes
15356000	Yukon R at Eagle, AK	0.008	−1	2.3	0.1	0.92	−0.06	0.07
15453500	Yukon R NR Stevens Village, AK	0.016	0	2.0	0.04	0.99	−0.02	0.02
15485500	Tanana R at Fairbanks, AK	0.1	0.8	−2.0	0.14	0.92	0.07	−0.02
15515500	Tanana R at Nenana, AK	0.014	−0.3	−0.8	0.07	0.98	−0.02	0.02
15565447	Yukon R at Pilot Station, AK	0.003	−1.00	1.9	0.15	0.80	−0.07	0.08
15875000	Colville R at Umiat, AK	0.200	1.20	12.5	0.16	0.98	0.34	−0.19
15908000	Sagavanirktok R NR Pump STA 3, AK	0.026	1.40	3.6	0.28	0.84	0.13	−0.09
	Mean	0.025	0.1	2.2	0.17	0.89	0.04	−0.01
	Stdev	0.037	0.7	5.2	0.18	0.32	0.14	0.11
	Max	0.200	1.4	20.9	0.79	1.00	0.58	0.37
	Min	0.001	−1.0	−3.4	0.03	−0.77	−0.15	−0.25
	Median	0.016	0.0	0.4	0.11	0.98	0.01	0.00
	75th	0.022	0.7	2.7	0.16	0.99	0.04	0.03
	25th	0.012	−0.4	−0.8	0.07	0.96	−0.03	−0.04
	Alaskan rivers							
	Mean	0.047	0.1	2.2	0.13	0.93	0.05	−0.02
	Stdev	0.069	0.9	4.7	0.07	0.07	0.13	0.09
	Max	0.200	1.4	12.5	0.28	0.99	0.34	0.08
	Min	0.003	−1.0	−2.0	0.04	0.80	−0.07	−0.19
	Median	0.015	0.0	1.9	0.12	0.95	0.01	0.00
	75th	0.045	0.9	2.7	0.15	0.98	0.09	0.03
	25th	0.011	−0.5	−1.1	0.08	0.90	−0.03	−0.05

n_b, bankfull reference Manning n; x, exponent of Manning n function; B, elevation of zero flow in channel (channel bottom); NRMSE, normalized root mean square error; NSE, Nash–Sutcliffe efficiency statistic; logRes, the log of the RSQ estimate minus the log of the observed discharge; PctRes, RSQ estimated discharge minus the observed discharge divided by the observed discharge; RSQ, remote sensing discharge.

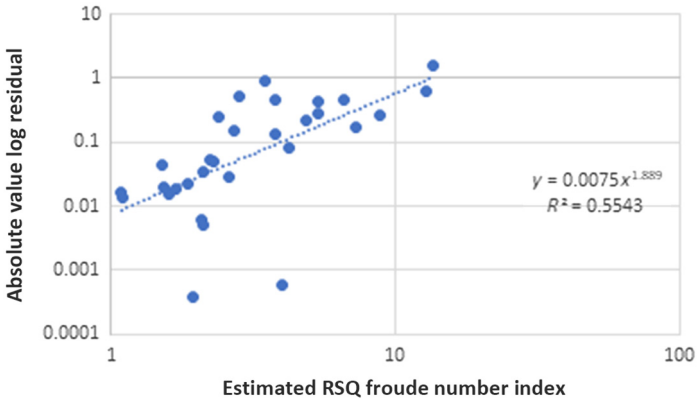

Fig. 10 Error as a function of Froude number index (F_{max}/F_{min}). RSQ, remote sensing discharge.

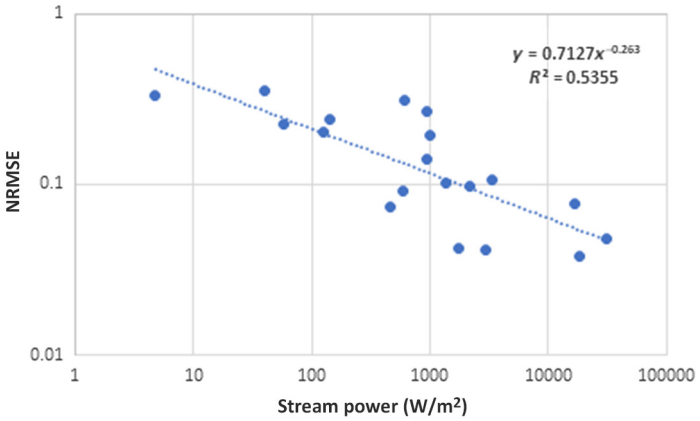

Fig. 11 Plot of the NRMSE against the Frasson et al.,[18,19] stream power.

The accuracy of space-based altimeters that track water-surface heights globally in general have reported observational accuracies (when compared to a time series of *in-situ* observations) of a few to several tens of cm reported as the root mean square (rms) error. The accuracy is dependent on many factors,[43] including the surface roughness and width, and is typically >10 cm rms for river reaches. For satellite-based laser altimeters, the accuracy is better and there is a greater potential to acquire stage for smaller tributaries.[75–77] There has been continuity of satellite radar altimeters over several decades but the latest radar altimeter missions, such as Sentinel-3 and Sentinel-6, use enhanced technology (Delay-Doppler SAR) in combination with innovative techniques such as fully-focused SAR (FF-SAR) with the aim of increasing the current spatial resolution of stage measurements along the ground, from 300 to 40–80 m.

Observations from the SWOT mission will be reported on a reach scale by averaging from a point cloud generated by wide swath altimetry (Biancamaria et al.[3] SWOT | PO.DAAC/JPL/NASA). The accuracy of the SWOT mission water surface heights and widths has not been fully evaluated as observational data is only beginning to be received. The accuracy of averaged water surface heights over a 10 km reach and 100 m wide river is expected to be on the order of 10 cm.[3] SWOT expected uncertainty in observations of water-surface width, expressed as the resolution of the image, is 15 m. Comparatively, Landsat resolution is 30 m,[39,40] however, the width accuracy is also a function of the classification algorithm that defines which pixels contain water. Although there are satellite-based imagers with much better resolution (10 m or better), these imagers do not routinely observe locations across the earth that can provide time series of observations. As such, it is expected that the best estimates of width observation uncertainty would be on the order of $+/-15$ m.

Bjerklie[26] showed that observational uncertainty—viewed as a fixed value for height and width (e.g., $+/-10$ cm for height and $+/-30$ m for width)—becomes more important in

Table 5 Error threshold statistics between observed and remote sensing estimated discharge (RSQ).

No. measurements	Fractional percent threshold	Fractional percent error of estimates below threshold	No. measurements	Fractional percent threshold	Fractional percent error of estimates below threshold
Fractional percent of measurements below error threshold for all data			Fractional percent of measurements below error threshold for all data		
1177	<0.05	0.39	1177	<0.05	0.39
1745	<0.1	0.58	1745	<0.1	0.58
2078	<0.15	0.69	2078	<0.15	0.69
Fractional percent of measurements below error threshold for depth > 2 m			Fractional percent of measurements below error threshold for discharge >1000 m^3/s		
938	<0.05	0.52	650	<0.05	0.65
1341	<0.1	0.74	883	<0.1	0.88
1519	<0.15	0.84	947	<0.15	0.95
Fractional percent of measurements below error threshold for depth > 3 m			Fractional percent of measurements below error threshold for discharge > 2000 m^3/s		
778	<0.05	0.63	559	<0.05	0.71
1071	<0.1	0.87	730	<0.1	0.92
1169	<0.15	0.95	765	<0.15	0.97

Fractional percent = Percent divided by 100; Fractional percent error = RSQ estimated discharge divided by measured discharge.

the overall accuracy of a discharge estimate as the river gets smaller. In other words, the effect of observation error becomes less important as rivers get larger because the uncertainty becomes a smaller percentage of the magnitude of the observed variable.

The reach lengths over which the averaging is accomplished may vary but fundamentally are constrained by the distances between satellite overpasses and the orientation of the river in relation to its intersection with the satellite crossing locations. Consequently, the impact of the reach on the average values is variable and somewhat unknown. Our assumption is that the reach averaging will not introduce substantial uncertainty provided the reach length is $> \sim 10$ rivers widths[78,79] and less than the distance between input tributaries. Uncertainty estimates of widths based on Landsat classification- were made through comparison with published ground-based values as well as those visually interpreted from finer-resolution satellite imagery collected coincidentally with the Landsat scenes being evaluated.[39,80] Estimates of uncertainty associated with satellite-based altimeters have been assessed by Birkett et al.[43] Bjerklie et al.[15] summarize these data sources and compare observations with ground observations for the Yukon River in Alaska.

Here we look at how WSE error propagates into the estimates generated from the discharge algorithm as presented in Eq. (3). It is assumed that $r = 2$ and the three parameters B, n_b, and x are calibrated. The discharge uncertainty is calculated from the derivative of Eq. (3) with respect to the change in height (dh) to characterize the sensitivity of the equation to the magnitude of h. Using uncertainty quantification methods, the uncertainty in discharge due to the WSE observations is

$$\sigma_Q^2 \approx \left(\frac{dQ}{dh}\right)^2 \sigma_h^2 + \left(\frac{dQ}{dW}\right)^2 \sigma_W^2, \tag{6}$$

where σ_Q is the discharge uncertainty due to WSE and width uncertainties, expressed as a standard deviation; σ_h and σ_W are the uncertainty standard deviation of WSE and width, respectively; and the derivatives represent the sensitivity of discharge to WSE and width, respectively. Equation (6) is approximate as it uses the first term in the Taylor series expansion of Q to represent the sensitivity of discharge to observations. The relation between the observations and river discharge is given by combining Eqs. (3) and (4). Differentiating the combined Eqs. (3) and (4), we use the law for derivative of a product to obtain

$$\begin{aligned}\frac{dQ}{dh} = {} & \frac{dn^{-1}}{dh} W \left[(h-B)\left(1-\frac{1}{1+r}\right)\right]^{1.67} S^{0.5} \\ & + 1.67\left(1-\frac{1}{1+r}\right)\frac{W}{n}\left[(h-B)\left(1-\frac{1}{1+r}\right)\right]^{0.67} S^{0.5},\end{aligned} \tag{7}$$

where the first term on the right-hand side of Eq. (7) is the derivative of n^{-1} and is given as

$$\frac{dn^{-1}}{dh} = \left[\frac{1}{n_b}\frac{1}{H-B} + \frac{x}{n_b}\frac{(H-B)^2}{(h-B)^3}\right] \exp\left(-x\left[\frac{H-B}{h-B}\right]\right). \tag{8}$$

Finally, the sensitivity of discharge to width is given as

$$\frac{dQ}{dW} = \frac{1}{n}\left[(h-B)\left(1-\frac{1}{1+r}\right)\right]^{1.67} S^{0.5}. \tag{9}$$

Thus, discharge uncertainty is computed by combining Eqs. (6)–(9). Relative discharge uncertainty can be computed by dividing the result by Manning's equation. One critical result that can be seen from the mathematics is that the derivatives are all a function of WSE themselves, and thus uncertainty changes with WSE; this is also true for the relative discharge uncertainty (not shown analytically). We explore the relative uncertainty by varying WSE and width values, along with width and WSE measurement uncertainty.

The resolution or uncertainty in the height observations for an example station on the Delaware River ranges from 1 to 15 cm, and the resolution or uncertainty in the width observations range from 5 to 15 m (Fig. 12). The uncertainty is far greater at low values of stage, and

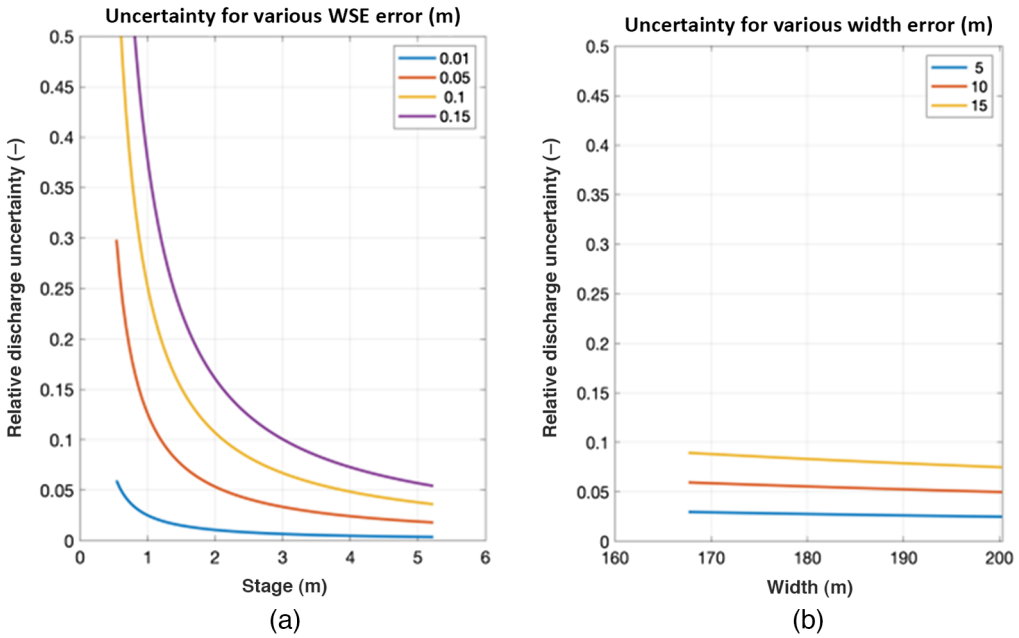

Fig. 12 Example of the effect of observation uncertainty on discharge uncertainty for the Delaware River data. (a) and (b) Discharge performance expressed as uncertainty as a function of the uncertainty in height and width observations, respectively.

thus at low flow (e.g., for a 10 cm WSE uncertainty) the relative discharge uncertainty is 40% at a stage of 1 m, but only 5% at a stage of 5 m. Note that the discharge uncertainty due to width is significantly lower, and furthermore is far less responsive to the width itself. These results emphasize the importance of considering discharge uncertainty at a range of flows. The absolute error in the discharge resulting from absolute error in stage (i.e., depth) and width is proportional, as shown by Bjerklie et al.,[26] because both width and stage are multiplicative elements discharge continuity (e.g., $Q = W * Y * V$). As such, the contribution of fixed error in width and stage becomes a larger proportion of observational error as the width, stage, and discharge become smaller.

Across all 30 rivers in the test data set, for 10 cm WSE error the 67th percentile of error yields relative discharge uncertainty of 12% at median flow (Fig. 13). At low flow, most rivers have

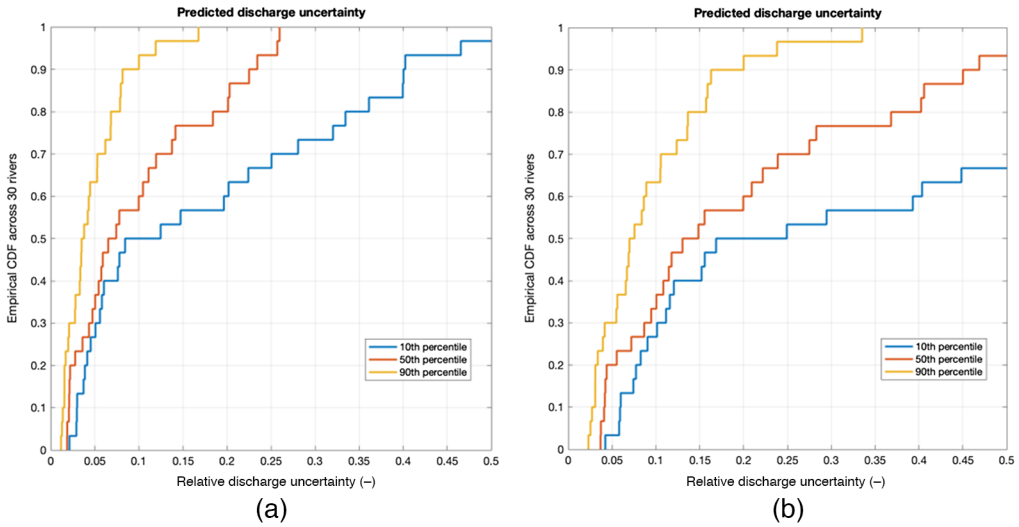

Fig. 13 Cumulative number of rivers (CDF) for the 30-river data set as a function of relative discharge uncertainty assuming (a) a 10 cm and (b) 20 cm uncertainty in WSE observations.

uncertainty <25%. A minority of rivers (90th percentile) are at a discharge uncertainty of 20% or greater at median flow. Increasing the WSE error to 20 cm makes a large change, with most rivers (67th percentile) now at 23% discharge error. Error in width shows much less impact across the 30 test rivers, as the assumed uncertainty in width observations does not constitute a large portion of the total width of the water-surface. Additionally, the width is smoothed to reduce random measurement error as previously discussed.

Assuming the error associated with the algorithm (model error) is on the order of 10%, for approximately half of the rivers the observation error is larger than the model error. For nearly all (85%) of the rivers, the error associated with the proxy satellite observations is a major or dominant component of overall error. Depth controls most of the variability and observation error dominates for shallower rivers. For some rivers, observation error is far greater than model error.

In summary, observation error will almost certainly remain a large part of the total discharge uncertainty in remote sensing of discharge. Even when error in the observation of WSE is <10 cm (which is a challenging goal) observation error will likely be greater than model error in most rivers. WSE uncertainty varies with river stage, increasing at low flow.

2.2.1 *Effect of slope and assumed regular cross-section (width) on discharge estimates*

Dynamic water-surface slope data were collected for the Tanana River near Fairbanks and used to evaluate the effect of dynamic slope compared to static slope on algorithm-derived discharge estimates. Unfortunately, there are few data sets available to provide a broader range of evaluation. The Tanana River water-surface height was monitored at three locations along the river reach that flows past the USGS streamgage at Fairbanks, AK (collected June 9–October 12, 2016; https://doi.org/10.5066/P9ZUUVPS). The height data was coupled with continuous discharge data at the gage to derive a data set of reach averaged change in height, slope, and discharge that spanned a several month period in 2016. Discharge estimates were derived from the height and slope observations and compared with the USGS estimates based on the stage-discharge rating curve at the gage (Fig. 14). The dynamic reach averaged width was not directly measured and as such it was estimated based on a relation between stage and width derived from observations of the maximum width and estimates of the bankfull depth, assuming that the river channel is parabolic in shape (see Bjerklie et al.[15]). This was accomplished by fitting a parabola with the width and depth defining the parabolic dimensions. The parabola is given as $Y = aW^2$ with Y being the depth and W the width. The coefficient a is set as the ratio of the bankfull depth, Y_b divided by the bankfull width, ${W_b}^2$, and the bankfull dimensions obtained from the discharge measurement record as previously described. Riggs et al.[13] have shown that reach averaged widths improve overall accuracy of discharge estimates compared to using a cross-section width, further supporting the value of width averaging. The assumption of a regular width derived from the stage also provides a means to test the importance of the accuracy of width in the discharge estimate algorithm.

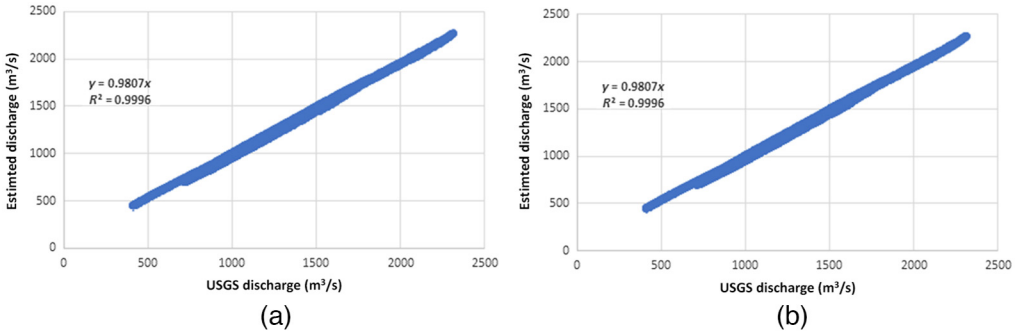

Fig. 14 (a) The estimated discharge versus the observed discharge over the summer of 2016 for the Tanana River at Fairbanks using the dynamic slope and assumed width and maximum depth. (b) The estimated discharge using a constant slope versus the discharge estimated using a dynamic slope only. USGS, U.S. Geological Survey.

Bjerklie et al.[26] have previously shown that assuming a constant slope does not degrade the overall accuracy of discharge estimates using a Manning flow resistance law compared to using measured dynamic slope. Similarly, the discharge estimates for the Tanana River derived from assuming a constant slope compared to a dynamic slope show only a small reduction in accuracy (on the order of 1% difference in overall mean). Additionally, the assumed width could be used to derive accurate discharge estimates through calibration, indicating that width can be viewed more or less as a scalar and need not necessarily be highly accurate compared to ground-measured width provided the estimates can be calibrated. These results indicate that initial values of discharge can be derived from appropriately scaled width and constant slope as a precursor to full dynamic observations of width and slope without significant degradation of estimate accuracy.

Additionally, the impact of using the measured width as opposed to a smoothed width that enforces a monotonic relation between stage and width is explored. In particular, the rivers that showed a relative nonlinear but regular pattern of stage versus width were recalibrated using the observed width rather than the smoothed width, and the results were compared. These rivers include the Susquehanna River at Marietta and Waverley, Delaware River, Connecticut River, Potomac, Wenatchee, Platte and the Tanana at Fairbanks.

The Tanana at Fairbanks is the only river that shows a stage width relation where the width increases more rapidly at a higher stage – interestingly this river produced a negative value of x for the two-parameter calibration, indicating that the rapid increase in width resulted in increasing flow resistance with increasing depth. Rerunning the calibration for these rivers using the observed width showed improvement in the mean log residual for several of the rivers including the Susquehanna at Marietta and Waverley, and the Platte with the NRMSE and the NSE remaining the same. The low-end bias for both Susquehanna stations also diminished indicating the value of a reliable observed reach averaged width where possible. However, given the present data set with width not measured consistently at the same location, the width smoothing is necessary. Additionally, width smoothing is necessary if stage and width are not measured at the same time.

2.3 *Parameter Uncertainty*

The Manning equation described by Eqs. (3) and (4) ingests measured variables of water-surface slope, water-surface width, and water-surface height. The Manning equation parameters that must be estimated for each river reach where the equation is applied include the bankfull and bottom reference heights (H and B) from which the water depth is referenced; the bankfull reference Manning n flow resistance (n_b), which is the reference point from which Manning n values at lower water-surface heights are referenced; the exponent x controls the variation of Manning n with respect to the relative depth; and the channel cross-section geometry coefficient r. As previously mentioned, we assume that the geometry coefficient is constant for all channels with a power of 2 (parabolic). Parameter errors are offset by averaging and calibration—minimizing the number of parameters to calibrate improves the overall accuracy of ground truth hydraulics and provides more reasonably accurate values for the mean velocity and depth.

2.3.1 *Manning* n*—flow resistance*

In many ways parameterizing the resistance coefficient poses the greatest potential for model error and may overwhelm the satellite measurement error in some rivers. Characterizing the value and the error associated with the Manning flow resistance over the entire range of flows in a river reach may be the greatest challenge associated with algorithm parameterization and warrants a more comprehensive understanding of what it represents (refer to Sec. 2.1 and the Appendix).

2.3.2 *Bankfull and channel bottom reference heights (H and B) and the linearity of the stage-width relation*

Key to the development of RSQ is the need to identify a robust relation between the average water-surface width and the WSE of the observed reach. This relation defines height as a

function of width from which an estimate B can be extrapolated. The setting of the bottom surface height (B) provides the reference for scaling the depth. The inverse relation, the width as a function of height, provides a linear forcing of the relation between width and height such that it is monotonic. This latter relation is essentially a width–height rating curve and acts to smooth observational irregularities between height and width due to measurement error and observational resolution under the assumption that height and width must increase at a concordant rate with discharge. Identification of a linear width–height relation may require more than one relation, if there are break points in the curve or if a shift has occurred in the channel as previously noted in Sec. 2.2.1. As previously noted in Sec. 2.2.1, this smoothing does not introduce a large amount of additional error in most cases; however, some rivers show improvement in the discharge estimates where the stage–width relation shows a marked break in slope. This points to the need for a robust quality assurance/quality control (QA/QC) of width measurements as part of assessment of accuracy.

3 Predicting Initial Parameter Values and Ranking the Expected Uncertainty of the Estimates for Each River Based on Diagnostic Characteristics

Developing a robust assessment of discharge estimate error for river reaches with no ground truth data for comparison will be very difficult given the range of assumptions, measurement error, and impact of calibration. As a result, we propose bracketing the estimates within an expected range of values derived from statistically based regime and flow relations that provide a "most probable state." The distance from this state would factor into the confidence in the potential accuracy of the estimate. The range of expected values is termed diagnostics. The Manning equation yields estimates of the discharge, mean depth, and mean velocity. These estimates can be compared to general ranges for these variables with associated hydraulic state variables (including the Froude number and the width-to-depth ratio) derived from statistical analysis of thousands of discharge measurements made by the USGS.[55] Additionally, bankfull hydraulic variables (regime variables) are estimated from a large data set of bankfull flow measurements in hundreds of rivers,[24] and the shape of the stage (height)-discharge rating curve considered in the diagnostics.

The following are the proposed diagnostic relations that can be used to define the likely or expected value for the estimated Froude number for each discharge estimate. As an assumption, the Froude number is expected to not exceed a value of 1,[67] and would be expected to be considerably below 1 in most cases especially considering that the choice of reach would avoid severe constrictions, hydraulic structures, and very steep slopes. The diagnostics can be applied to the estimated bankfull (regime) flow conditions including the bankfull depth (Y_b) and Froude number (F_b), The diagnostic estimating equations are found in Refs. 24 and 15. The bankfull estimate is critical for providing the reference point for scaling the Manning n and the depth. If the values fall within the range predicted by the 95% confidence interval for Y_b and F_b there would be high confidence in the estimate. There would be low confidence if the estimate was outside the 95% range. Values of Manning n are also checked against the expected range of values as found in various literature reviews.[61,62,81,82]

We rely on bankfull diagnostics with the understanding that the bankfull state—including width, depth, velocity, meander length,[24] slope, and discharge are not precise values, and in fact, may vary over time (often over short time periods). Consequently, we view these diagnostics as important scaler quantities that form an expected state as a means to understand the likelihood that the estimated values are within the expected range.

Bankfull velocity based on meander length (L) and slope (S) with 95% confidence range[24]

$$\begin{aligned} V_b &= 1.37 \times (L)^{0.31}(S)^{0.32} \text{ mean} \\ V_b &= 1.00 \times (L)^{0.30}(S)^{0.26} \text{ lower } 95\% \\ V_b &= 1.88 \times (L)^{0.34}(S)^{0.37} \text{ upper } 95\%, \end{aligned} \tag{10}$$

$$V_b = 2.38 \times (\mathrm{LS})^{0.5}, \tag{11}$$

from Jansen et al.[63]

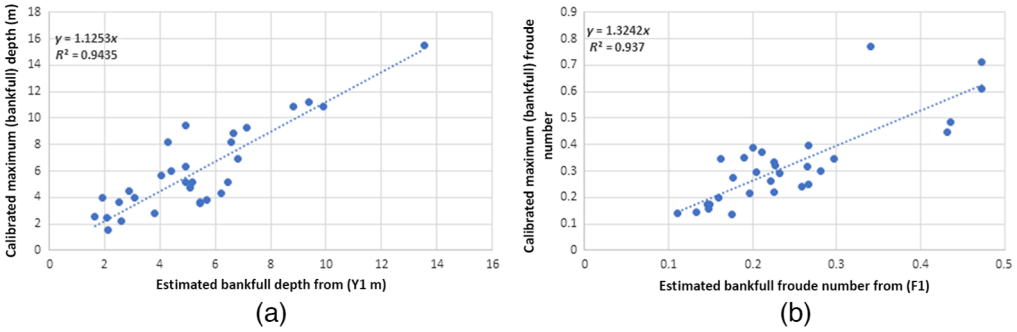

Fig. 15 Comparison of calibrated versus diagnostic estimates of bankfull depth (maximum in channel) from Eq. (12) (a) and Froude number from Eq. 13 (b) for the 30-river data set.

Bankfull Depth based on bankfull width (W) and slope (S) with 95% confidence range[24]

$$\begin{aligned} Y_b &= 0.08 \times W^{0.39} S^{-0.24} \text{ mean} \\ Y_b &= 0.07 \times W^{0.34} S^{-0.28} \text{ lower } 95\% \\ Y_b &= 0.10 \times W^{0.43} S^{-0.20} \text{ upper } 95\%. \end{aligned} \tag{12}$$

Bankfull Froude Number based on slope (S) with 95% confidence range[15]

$$F_b == 2.85 \times S^{0.31} \text{ mean}, \tag{13}$$

where $F = \frac{V}{\sqrt{gY}}$, $F_b == 2.34 \times S^{0.28}$ lower 95%, $F_b == 3.47 \times S^{0.34}$ upper 95%.

Relations between estimated and calibrated bankfull depths and Froude numbers indicate *a priori* estimates of the bankfull depth and Froude number can be used to provide initial algorithm parameters (Fig. 15).

Additional hydrologic information may help to understand uncertainty as well as constrain parameter estimates. The hydrologic conditions within the watershed, either compiled from published sources (e.g., USGS Gages-II database[83]) or derived using a GIS, can help differentiate rivers with higher and lower uncertainty as measured by the NRMSE.[69] Rivers with calibrated NRMSE < 10% are clearly distinguished from those with NRMSE > 10% as a function of the number of dams in the watershed (dam density) and as a function of the baseflow index (BFI) (Fig. 16).

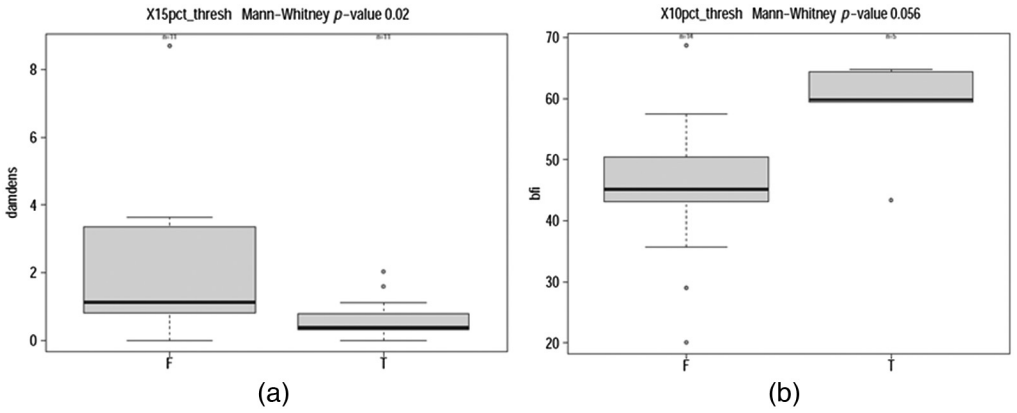

Fig. 16 Box plots showing the differentiation between rivers with mean normalized root mean square error (NRMSE) (a) greater (F) and lesser (T) than 15% as a function of dam density (dams per 100/km^2 labeled damdens) and (b) greater and lesser than 10% as a function of baseflow index (labeled BFI). The thick line is the median value in each box bounded by the 25th and 75th quartiles, with whiskers denoting 1.5 times the interquartile range above and below the median, and outliers are denoted as points.

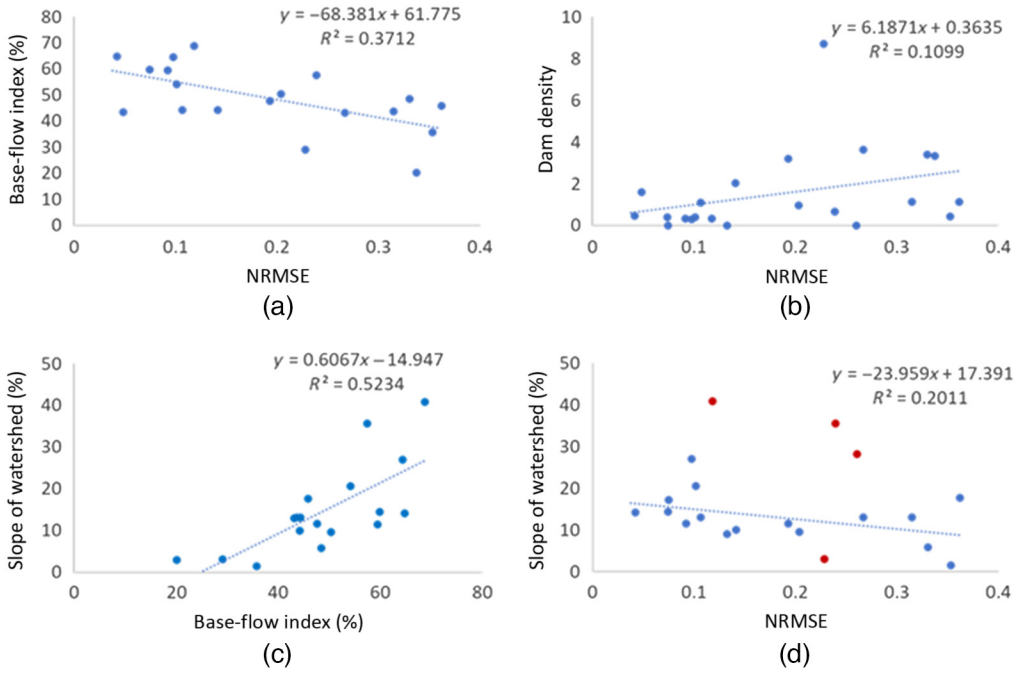

Fig. 17 Various hydrologic aspects of the watershed can be used to predict expected error in RSQ. (a) Expected error (normalized root mean square error, NRMSE) increases as baseflow decreases and (b) dam density increases. (c) Average basin slope is well correlated to base-flow index (BFI) and provides a more readily available metric. (d) Expected error increases as average slope in the watershed decreases. Sites in red are excluded from the linear regression due to their extreme slope values and small drainage basins.

BFI is the ratio of volumetric ground-water discharge to a stream (baseflow) to total volumetric streamflow. Values were obtained for select USGS gage test sites[83] or derived using a BFI raster[84] in ArcGIS as the average BFI within a drainage basin. BFI and NRMSE are negatively correlated ($R^2 = 0.37$), indicating sites with higher groundwater supply to a stream and/or low-flow dam releases from upstream and generally lower total streamflow, experience a higher error in estimated discharge. Baseflow and dam density provide useful metrics for predicting model performance (Fig. 16); however, readily accessible BFI datasets[83,84] are only available for the conterminous United States. Assessing metrics with known relationships to BFI and damn density can provide a useful substitute in areas outside of the conterminous United States.

A positive relationship between baseflow and average slope in the watershed has been demonstrated in various studies although it is less clear if increased basin slope drives increased baseflow.[85,86] Average watershed slopes for the test sites were obtained from Gages-II[83] or derived in ArcGIS Pro using 30-m resolution DEM from the USGS National Map data delivery.[87] A positive correlation between BFI and average basin slope is observed at the test sites ($R^2 = 0.52$, Fig. 17); however, a much weaker negative correlation is observed between NRMSE and average basin slope ($R^2 = 0.08$). There are a few sites with extremely high slopes (slope $> 35\%$; Snohomish River near Monroe, WA; Sagavanirktok River near Pump Station 3, AK; Wenatchee River at Monitor, WA) and low slopes (slope $< 5\%$; Neuse River near Clayton, NC; Platte River near Agency, MO). These sites have the smallest drainage areas in the test dataset, and therefore their average slope is more sensitive to changes in topography. If these five sites are removed, the negative correlation between the average basin slope and NRMSE becomes stronger ($R^2 = 0.20$, Fig. 17).

Expected error in RSQ increases as flow becomes more regulated, shown through the increase in NRMSE as dam density increases ($R^2 = 0.11$, Fig. 17). Dam density is the number of dams in the watershed per 100 km^2 and was obtained for select USGS gage sites[83] or derived in ArcGIS using the U.S. Army Corps of Engineers *National Inventory of Dams* online Feature Service hosted by Esri US Federal Data on ArcGIS Online.

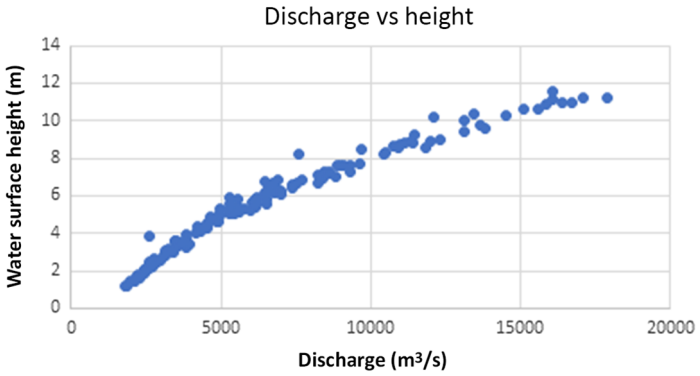

Fig. 18 Measurement data for the Mississippi River at Thebes Illinois showing the relationship between discharge and water-surface height (the stage-discharge rating curve).

Additional diagnostics are based on the shape of the rating curve derived from the discharge estimates and the WSE. The form of the rating curve based on general theoretical considerations must be convex (e.g., cross-sectional area of flow and velocity increase with increasing discharge) to some degree. One exception might be if the flow becomes super-critical, which is not common in natural rivers.[67] This means that discharge cannot decrease with increasing stage. The shape serves as an indicator of the physical reality of the discharge estimates. Natural rivers demonstrate a convex rating curve between height as a function of discharge,[88] as shown below for the Mississippi river (Fig. 18). The reason for this is based on continuity and the fact that the river is an open channel—as stage increases so does the cross-sectional area of flow and hydraulic radius, and thus discharge must also increase. This is based on the assumption that the discharge cannot decrease below what the discharge was prior to stage increase, which is not necessarily true if the slope is changing due to hysteresis (changing slope during rising and falling limb of a flood wave). This study does not attempt to evaluate the effects of hysteresis because the interval between satellite repeat observations is too long to capture the rapid dynamics of the flood wave moving downstream, the reach length may exceed the flood wavelength, and the Manning equation is not suited for rapidly varied flow conditions.[48] Mean velocity in the cross-section may decrease in some situations as stage increases because as stage increases additional roughness from vegetation and large obstructions (e.g., boulders) are encountered on the banks and on side bars or additional channels are occupied (as in the case of braided channels), or in rivers where the rate of increase in width increases faster than the rate of increase in WSE.

3.1 *Overall Uncertainty*

Considering the uncertainty associated with the algorithm, calibrated parameters, and measurement error, it is possible to develop a general understanding of expected uncertainty (accuracy) in the discharge estimates depending on flow regime. Combining the expected algorithm and parameter estimation accuracy for a well calibrated model, we would expect accuracy on the order of 10% of USGS ground-based values of discharge and a general input variable measurement accuracy on the order of 10% (primarily measurement errors associated with WSE). With these assumptions, the overall expected uncertainty would be ~14% for most rivers using

$$x = \sqrt{E1^2 + E2^2}, \tag{14}$$

where $E1$ is the uncertainty due to the algorithm and parameter estimates, and $E2$ is the uncertainty due to input variable measurement error.

For rivers with a wide range of estimated Froude numbers and shallow slopes, as well as rivers with high BFI and impacts from dams, the accuracy would decrease due to algorithm and parameter uncertainty such that the expected algorithm uncertainty would increase up to 20% or more even as measurement accuracy remains the same at 10%. Thus, according to Eq. (10) the general expected accuracy would be on the order of 22%.

However, as has been demonstrated, for most rivers the uncertainty associated with the algorithm and parameter estimation as well as input data measurements increases significantly for shallower depths (<3 m) and lower discharge (<1000 m^3/s). Thus, it can be said that as discharge and depth decrease, uncertainty increases especially for those rivers that have shallow slopes, are impacted by dams, and have a high BFI. The low discharge and shallow depth uncertainty may increase to 50% or more and at higher flows and depths uncertainty is significantly lower, which is key to understanding and applying the RSQ flow data.

In the context of an accuracy classification system the expectation would be that an RSQ gage on a large river that is well calibrated (10 to 20 calibration points) and meets the assumptions of the flow law algorithm that is free of dams has a low BFI range of Froude numbers, and a relatively steep slope would have good to fair discharge ratings (15% or less uncertainty). Smaller rivers that do not meet the assumptions of the flow law algorithm, show a wide range in Froude numbers, have relatively shallow slopes, have a relatively high BFI, and are impacted by dams, would be expected to have fair to poor discharge ratings (15% or greater uncertainty).

4 Summary and Conclusions

Based on the results found in the application summarized here, average RSQ estimates for any given river reach may be expected to have an uncertainty associated with the flow law model in the range of 10% overall for most rivers given an adequate number of calibration points. This would represent the uncertainty associated with the general algorithm that is presented. Uncertainty may be reduced by using the nonlinear Manning n transformation [Eq. (15)] and if width observations are reliable and coincident with the observations of stage, which will be the case with data coming from the SWOT mission, scheduled to launch in December 2022.

Comparing the five error objective functions considered in this paper (NRMSE, KGE, NSE, log residual, and percent residual) it is found that the KGE and NSE are highly correlated and provide a similar analysis of the combined accuracy and dynamics of the estimates. The mean of the log residual and the percent residual is also well correlated although often with opposite signs, suggesting that these two measures provide similar information on the error also. The NRMSE is not as well correlated with the other measures, indicating that it provides a uniquely different perspective of error. None of the direct measures of error (logRes, pctRes, and NRMSE) are well correlated with either the NSE or KGE. Overall, given the generally very good NSE and KGE values, it can be surmised that the dynamics are well captured by the algorithm because of the dynamic response of the WSE.

The number of adequate calibration points is considered to be <20 observations for most rivers, with the mean and median converging to a stable KGE with six calibration points. The error and uncertainty in the algorithm increase markedly for depths <3 m and at the low end of discharge (<1000 m^3/s) for many rivers even after calibration. Some improvement in the algorithm performance, with less overall uncertainty and less uncertainty at the low end of discharge can be achieved using a non-linear Manning n transformation function.

Application of the discharge algorithm at river reaches with favorable characteristics is an important qualifier. This study indicates that rivers with a wide range of Froude numbers (ratio of maximum to minimum Froude number in the simulated record), have a significant number of dams in the watershed and along the channel, and rivers exhibiting a high BFI are more likely to have relatively large errors overall and particularly at the low end of the flow range. For rivers that have a wide range of flow conditions with many discharge estimates below 1000 m^3/s and depths < 3 m, it is recommended that the non-linear Manning transformation function be used [Eq. (5)]. Although defining characteristics of the river reach including sinuosity, meander length, valley slope, channel shape, etc. have not been specifically addressed in this study, on-going investigations are working toward a more robust representation of the river reach geometry for predicting discharge parameters.

Uncertainty associated with remote-sensing measurements in the expected range (WSE 10 cm and Width 15 m) introduces ~10% to discharge estimates and is greatest at the low end of discharge as rivers get shallower and narrower. If measurement uncertainty increases, discharge uncertainty increases accordingly. Error in the measurement of WSE is key to evaluating the magnitude of expected uncertainty in the discharge estimates. In general, the observation

errors will be greater than the errors associated with the algorithm for a well calibrated model (e.g., 20 calibration points).

Given adequate calibration with a measured bottom depth (B), the estimates of depth and velocity yield realistic values for the hydraulic state of flow, as indexed by the Froude number indicating that the estimates can also be used to assess changes in velocity and depth as discharge changes, extending the potential for applications of the RSQ estimates.

Expected uncertainty, ranked low, moderate, or high (accuracy good, fair, poor) can be evaluated as a function of hydrologic aspects of the watershed, and the range of depths and velocities in the estimated flow. Estimated discharge error is expected to increase as BFI decreases, average basin slope decreases, or dam density increases. Where calibration data are not available, RSQ algorithm parameters can be estimated *a priori* using diagnostic relations. Although this study does not address remote-sensing based estimates of overbank discharge (floods), it can be surmised that uncertainty of flood estimates would be larger than for in-bank discharge because of the increased complexity and difficulty in evaluating overbank flow resistance.

This paper presents an initial understanding of the error characteristics that would be expected from the application of a flow resistance equation to model the dynamic discharge in a wide range of rivers in diverse environments. This is an important consideration for many potential applications where known accuracy would be critical. The largest source of uncertainty in the model parameterization is likely to be the flow resistance in any given reach, and this can vary significantly from reach to reach and with flow level. The use of a flow resistance-based model can yield realistic hydraulic characteristics of the flow if flow resistance is properly characterized and flow depth reasonably approximated. The study also shows that higher accuracy of discharge estimates can be expected in larger, deeper, and unregulated rivers. This latter result indicates that flow resistance becomes more predictable in larger rivers and points to the advantageous use of remote sensing-based gaging stations on larger rivers. Additionally, this study has shown that fewer than ten ground-based discharge measurements may be sufficient to calibrate a river discharge gage especially on larger rivers, further indicating that limited resources may be diverted to smaller rivers and streams.

Additional suggestions for the development of satellite-based streamflow gaging stations include the use of methods (1) that can incorporate various sources of RS observations to create greater temporal density, (2) that are hydraulically based (such as a flow resistance equation) that can incorporate and be calibrated with velocity observations should they become available. Given the dependency of accuracy on the size of the river, incorporating RSQ estimates into existing ground-based streamflow gage networks can reduce the number of ground-based measurements needed on larger rivers enabling the redeployment of ground-based resources to gages on smaller streams and rivers.

5 Appendix

The Chezy equation can be derived by assuming that the gravitational forces driving the flow (the channel slope) is balanced by the shearing forces at the boundary (friction and drag).[89]

$$\tau = a\rho v^2, \tag{15}$$

where τ is the shear stress on the boundary expressed as a function of the velocity of flow, v, and ρ is the mass density of the fluid. The constant a relates the velocity of the fluid to the resisting shear forces at the bed and is assumed to represent the effects of friction and drag forces outside of the turbulent boundary layer. Drag theory states that in fully turbulent flow, the viscous boundary layer is small, and the effective velocity is zero at the boundary, with viscous shearing (frictional) forces within the fluid decreasing as a function of distance from the boundary hence the velocity increases as shear decreases away from the boundary.[48,90] For any given state of flow, the value of the constant a is related to the elements in the flow field that resist flow and create shear including friction associated with boundary roughness and boundary material.

The reduction in shear away from the boundary is primarily due to a reduction in the normal pressure exerted by the weight density (γ) of the fluid at the bed with decreasing depth of water above the point of interest.[48,51,89] The depth is represented by the hydraulic radius, R, which is

the cross-sectional area divided by the wetted perimeter of flow, and for wide channels is approximately the same as the mean depth of flow, which is the cross-sectional area divided by the top width of flow. Thus, shearing force can also be equated to R and the channel slope, S, (the frictional surface) of the bed, given by Eq. (16) where the variable S is the energy slope of the flow reach

$$\tau = \gamma \mathrm{RS}. \tag{16}$$

Equating Eqs. (15) and (16) yields

$$v = \sqrt{\frac{g\mathrm{RS}}{a}}, \tag{17}$$

where g is the gravitational constant (9.8 $\mathrm{m/s^2}$ in SI units), which is a constant for applications on the earth's surface. Taking the constants outside of the radical and defining a new constant C Eq. (18) yields the Chezy Eq. (19) for steady uniform flow in a conduit or channel with V is the mean velocity, R is the hydraulic radius (cross-sectional area divided by the wetted perimeter of the cross-section), and C is the Chezy coefficient.

$$C = \sqrt{\frac{g}{a}}, \tag{18}$$

$$V = C\sqrt{\mathrm{RS}}. \tag{19}$$

Robert Manning[48,89] empirically estimated the Chezy coefficient such that

$$C = \frac{R^{0.17}}{n}, \tag{20}$$

where n is the Manning resistance coefficient.

Substituting Eq. (20) into Eq. (19) results in the Manning equation

$$V = \frac{R^{0.67} S^{0.5}}{n}. \tag{21}$$

Acknowledgements

The research presented in this paper has been funded by the NASA Applied Sciences Program and the USGS Next-Generation Water Observing System. For more information, visit.[91] Any use of trade, firm, or product names is for descriptive purposes only and does not imply endorsement by the U.S. Government.

References

1. M. Khaki et al., "Multi-mission satellite remote sensing data for improving land hydrological models via data assimilation," *Sci. Rep.* **10**, 18791 (2020).
2. X. Xu et al., "Progress in integrating remote sensing data and hydrologic modeling," *Prog. Phys. Geog.* **38**, 464–498 (2014).
3. S. Biancamaria, D. P. Lettenmaier, and T. M. Pavelsky, "The SWOT mission and its capabilities for land hydrology," *Surv. Geophys.* **37**, 307–337 (2016).
4. National Aeronautics and Space Administration (NASA), "Surface water and ocean topography (SWOT) mission," http://swot.jpl.nasa.gov/mission/ (accessed 31 May 2022).
5. J. E. Kiang et al., "A comparison of methods for streamflow uncertainty estimation," *Water Resour. Res.* **54**, 7149–7176 (2018).
6. C. J. Gleason and L. C. Smith, "Toward global mapping of river discharge using satellite images and at-many-stations hydraulic geometry," *PNAS* **111**(13), 4788–4791 (2014).
7. S. J. Birkinshaw et al., "Using satellite altimetry data to augment flow estimation techniques on the Mekong River," *Hydrol. Processes* **24**(26), 3811–3825 (2010).

8. S. J. Birkinshaw et al., "Daily discharge estimation at ungauged river sites using remote sensing," *Hydrol. Processes* **28**(3), 1043–1054 (2014).
9. M. Durand et al., "Estimating reach-averaged discharge for the River Severn from measurements of river water-surface elevation and slope," *J. Hydrol.* **511**(C), 92–104 (2014).
10. P.-A. Garambois and J. Monnier, "Inference of effective river properties from remotely sensed observations of water surface," *Adv. Water Resour.* **79**, 103–120 (2015).
11. M. Durand et al., "An intercomparison of remote sensing river discharge estimation algorithms from measurements of river height, width, and slope," *Water Resour. Res.* **52**, 4527–4549 (2016).
12. M. G. Bonnema et al., "Benchmarking wide swath altimetry-based river discharge estimation algorithms for the Ganges river system," *Water Resour. Res.* **52**, 2439–2461 (2016).
13. R. M. Riggs et al., "RODEO: an algorithm and Google Earth Engine application for river discharge retrieval from Landsat," *Environ. Model. Software* **148**, 105254 (2022).
14. R. P. D. M. Frasson et al., "Exploring the factors controlling the error characteristics of the Surface Water and Ocean Topography mission discharge estimates," *Water Resour. Res.* **57**, e2020WR028519 (2021).
15. D. M. Bjerklie et al., "Satellite remote sensing estimation of river discharge: application to the Yukon River Alaska," *J. Hydrol.* **561**, 1000–1018 (2018).
16. R. P. D. M. Frasson et al., "Automated river reach definition strategies: applications for the surface water and ocean topography mission," *Water Resour. Res.* **53**, 8164–8186 (2017).
17. T. A. Cohn, J. E. Kiang, and R. R. Mason, "Estimating discharge uncertainty using the interpolated variance estimator," *J. Hydraul. Eng.* **139**(5), 502–510 (2013).
18. R. P. D. M. Frasson et al., *Global Database of River Width, Slope, Catchment Area, Meander Wavelength, Sinuosity, and Discharge [Data set]*, Zenodo (2019).
19. R. P. D. M. Frasson et al., "Global relationships between river width, slope, catchment area, meander wavelength, sinuosity, and discharge," *Geophys. Res. Lett.* **46**, 3252–3262 (2019).
20. I. Fujita et al., "Efficient and accurate estimation of water surface velocity in STIV," *Environ. Fluid Mech.* **19**, 1363–1378 (2019).
21. A. Kääb, B. Altena, and J. Mascaro, "River-ice and water velocities using the Planet optical CubeSat constellation," *Hydrol. Earth Syst. Sci.* **23**, 4233–4247 (2019).
22. C. J. Legleiter and P. J. Kinzel, "Field measurements of flow velocity and optical image sequences acquired from the Salcha and Tanana Rivers in Alaska in 2018 and 2019 and used for particle image velocimetry (PIV)," U.S. Geological Survey data release (2020).
23. C. M. Birkett, D. Alsdorf, and D. Harding, "Estimation of River and Water Body stage, width and gradients using Radar Altimetry, Interferometric SAR and Laser Altimetry, Volume 2 Part 5 (Remote Sensing) chapter 60," in *The Encyclopedia of Hydrological Sciences*,M. G. Anderson, Ed., John Wiley & Sons Ltd. Chichester, UK (2005).
24. D. M. Bjerklie, "Estimating the bankfull velocity and discharge for rivers using remotely sensed river morphology information," *J. Hydrol.* **341**(3–4), 144–155 (2007).
25. D. M. Bjerklie et al., "Estimating discharge in rivers using remotely sensed hydraulic information," *J. Hydrol.* **309**, 191–209 (2005).
26. D. M. Bjerklie et al., "Evaluating the potential for measuring river discharge from space," *J. Hydrol.* **278**(1–4), 17–38 (2003).
27. G. R. Brakenridge et al., "Orbital microwave measurement of river discharge and ice status," *Water Resour. Res.* **43**, W04405 (2007).
28. S. L. Dingman and D. M. Bjerklie, "Hydrological application of remote sensing: surface fluxes and other derived variables-river discharge," in *Encyclopedia of Hydrological Sciences*, M. G. Anderson and J. J. McDonnell, Eds., pp. 5–61, John Wiley and Sons (2006).
29. G. LeFavour and D. Alsdorf, "Water slope and discharge in the Amazon River estimated using the shuttle radar topography mission digital elevation model," *Geophys. Res. Lett.* **32**, L17404 (2005).
30. J. G. Leon et al., "Rating curves and estimation of average water depth at the upper Negro River based on satellite altimeter data and modeled discharges," *J. Hydrol.* **328**(3–4), 481–496 (2006).
31. L. C. Smith et al., "Estimation of discharge from three braided rivers using synthetic aperture radar satellite imagery," *Water Resour. Res.* **32**(7), 2021–2034 (1996).

32. L. C. Smith, "Satellite remote sensing of river inundation area, stage, and discharge: a review," *Hydrol. Processes* **11**, 1427–1439 (1997).
33. P. Lin et al., "Global reconstruction of naturalized river flows at 2.94 million reaches," *Water Resour. Res.* **55**(8), 6499–6516 (2019).
34. B. Brinkerhoff et al., "Constraining remote river discharge estimation using reach-scale geomorphology," *Water Resour. Res.* **56**, e2020WR027949 (2020).
35. C. M. Birkett et al., "Surface water dynamics in the Amazon Basin: application of satellite radar altimetry," *J. Geophys. Res.* **107**(D20), 8059 (2002).
36. C. M. Birkett and B. Beckley, "Investigating the performance of the Jason-2/OSTM radar altimeter over Lakes and Reservoirs, Jason-2/OSTM Special Issue," *Mar. Geod.* **33**(1), 204–238 (2010).
37. S. Calmant et al., "Amazon River stages by ENVISAT vs. other satellite altimeters, poster session 4P12-02 "Lake Levels," in *Abstract 671, 2004 ERS and ENVISAT Symp.*, Salzburg (2004).
38. M. Carroll et al., "Quantifying surface water dynamics at 30 meter Spatial resolution in the North American high northern latitudes 1991–2011," *Remote Sens.* **8**(8), 622 (2016).
39. J. W. Jones, "Efficient wetland surface water detection and monitoring via Landsat: comparison with in-situ data from the Everglades Depth Estimation Network," *Remote Sens.* **7**(9), 12503–12538 (2015).
40. J. W. Jones, "Improved automated detection of subpixel-scale inundation—revised Dynamic Surface Water Extent (DSWE) partial surface water tests," *Remote Sens.* **11**(4), 374 (2019).
41. J.-W. Kim et al., "Monitoring Everglades freshwater marsh water level using L-band synthetic aperture radar backscatter," *Remote Sens. Environ. B.* **150**, 66–81 (2014).
42. M. G. Tulbure and M. Broich, "Spatiotemporal dynamic of surface water bodies using Landsat time-series data from 1999 to 2011," *ISPRS J. Photogramm. Remote Sens.* **79**, 44–52 (2013).
43. C. Birkett, M. Ricko, and X. Yang, "Stream stage measurements: V2.5.1 water level products from Satellite Radar Altimetry," NASA/TM-20205011785 Algorithm Theoretical Basis Document (ATBD) (2021).
44. V. B. Sauer and D. P. Turnipseed, Stage Measurement at Gaging Stations, U.S. Geological Survey Techniques and Methods book 3, chap, **A7**, 45 p. (2010)
45. D. P. Turnipseed and V. B. Sauer, *Discharge Measurements at Gaging Stations*, book 3, chap. A8, 87 p., U.S. Geological Survey Techniques and Methods (2010).
46. Y. Yoon et al., "Presentation, evaluation and sensitivity of a discharge algorithm for remotely sensed river measurements: test cases on Sacramento and Garonne Rivers," *Water Resour. Res.* **52** (1), 278–294 (2016).
47. S. Tuozzolo et al., "Estimating river discharge with swath altimetry: a proof of concept using AirSWOT observations," *Geophys. Res. Lett.* **46**, 1459–1466 (2019).
48. V. T. Chow, *Open-Channel Hydraulics*, McGraw-Hill Civil Engineering Series, New York, pp. 680 (1959).
49. C. J. Gleason, P.-A. Garambois, and M. T. Durand, "Tracking river flows from space," *Eos* **98** (2017).
50. C. J. Gleason and M. T. Durand, "Remote sensing of river discharge: a review and a framing of the discipline," *Remote Sens.* **12**, 1107 (2020).
51. S. L. Dingman, *Fluvial Hydraulics*, p. 559, Oxford University Press (2009).
52. J. C. Blodgett, "Rock riprap design for protection of stream channels near highway structures, Volume 1—Hydraulic characteristics of open channels," U.S. Geological Survey Water-Resources Investigations Report 86-4127, 60 p. (1986).
53. T. H. Havelock, "The effect of shallow water on wave resistance," *Proc. R. Soc. Lond. A* **100**, 499–505 (1922).
54. S. Prakash and B. Chandra, "Numerical estimation of shallow water resistance of a river-sea ship using CFD," *Int. J. Comput. Appl.* **71**, 33–40 (2013).
55. D. M. Bjerklie et al., "Fundamental hydraulics of cross sections in natural rivers: preliminary analysis of a large data set of acoustic Doppler flow measurements," *Water Resour. Res.* **56**, e2019WR025986 (2020).

56. D. D. Franz and C. S. Melching, "Full equations utilities (FEQUTL) model for the solution of the full, dynamic equations of motion for the approximation of hydraulic characteristics of open channels and control structures during unsteady flow," U.S. Geological Survey Water Resources Investigations Report 97-4037 (1997).
57. D. M. Hicks and P. D. Mason, Roughness Characteristics of New Zealand Rivers, pp. 329, New Zealand DSIR Marine and Freshwater Resources Survey, Wellington (1998).
58. D. M. Powell, "Flow resistance in gravel-bed rivers: progress in research," *Earth Sci. Rev.* **136**, 301–338 (2014).
59. E. Rodriguez, M. Durand, and R. P. D. M. Frasson, "Observing rivers with varying spatial scales," *Water Resour. Res.*, **56**, e2019WR026476 (2020).
60. K. Blanckaert and H. J. de Vriend, "Meander dynamics: a nonlinear model without curvature restrictions for flow in open-channel bends," *J. Geophys. Res.* **115** (2010).
61. L. De Doncker et al., "Determination of the Manning roughness coefficient influenced by vegetation in the river Aa and Biebrza river," *Environ. Fluid Mech.* **9**, 549–567 (2009).
62. P. Gualtieri et al., "Use of conventional flow resistance equations and a model for the Nikuradse roughness in vegetated flows at high submergence," *J. Hydrol. Hydrmech.* **66**(1), 107–120 (2017).
63. P. Jansen et al., *Principles of River Engineering*, p. 509, Pitman (1979).
64. L. B. Leopold et al., *Flow Resistance in Sinuous or Irregular Channels*, Prof. Paper 282-D, 134 p., US Geological Survey (1960).
65. W. F. Coon, "*Estimation of Roughness Coefficients for Natural Stream Channels with Vegetated Banks*, Water Supply Paper 2441, p. 133, U.S. Geological Survey (1998).
66. R. Ferguson, "Flow resistance equations for gravel- and boulder-bed streams," *Water Resour. Res.* **43**, W05427 (2007).
67. G. Grant, "Critical flow constraints flow hydraulics in mobile-bed streams: a new hypothesis," *Water Resour. Res.* **33**(2), 349–358 (1997).
68. U.S. Geological Survey, "USGS Water Data for the Nation," U.S. Geological Survey National Water Information System database, accessed on various dates at https://doi.org/10.5066/F7P55KJN (2022).
69. J. M. LeNoir, D. M. Bjerklie, and R. W. Dudley, *Data from Across the USA Used to Assess the Uncertainty of Discharge Estimates Using a Modified Manning's Equation*, U.S. Geological Survey, data release (2022).
70. H. V. Gupta et al., "Decomposition of the mean squared error and NSE performance criteria: implications for improving hydrological modeling," *J. Hydrol.* **377**(1–2), 80–91 (2009).
71. J. Wouter et al., "Technical note: inherent benchmark or not? Comparing Nash-Sutcliffe and Kling-Gupta efficiency scores," *Hydrol. Earth Syst. Sci.* **32**, 4323–4331 (2019).
72. J. E. Nash and J. V. Sutcliffe, "River flow forecasting through. Part I. A conceptual models discussion of principles," *J. Hydrol.* **10**, 282–290 (1970).
73. D. Rickenmann and A. Recking, "Evaluation of flow resistance in gravel-bed rivers through a large field data set," *Water Resour. Res.* **47**, W07538 (2011).
74. S. L. Dingman and K. P. Sharma, "Statistical development and validation of discharge equations for natural channels," *J. Hydrol.* **199**, 13–35 (1997).
75. C. M. Birkett et al., "Application of ICESat/ GLAS laser altimetry to the estimation of Surface Water Level and River Discharge," presented at *The 2010 Fall Meeting*, AGU, San Francisco, California, 13-17 Dec., Abstract C43F-02 (2010).
76. M. F. Jasinski et al., ATLAS/ICESat-2 L3B mean inland surface water data, Version 2, NASA Goddard Space Flight Center, Greenbelt, Maryland (2021a).
77. M. F. Jasinski et al., *Algorithm Theoretical Basis Document (ATBD) for Mean Inland Surface water data ATL22, Release 2*, 40 pp., National Snow and Ice Data Center, Boulder Co. (2021b).
78. C. W. Carlston, "The relation of free meander geometry to stream discharge and its geomorphic implications," *Am. J. Sci.* **263**, 864–885 (1965).
79. G. P. Williams, "River meanders and channel size," *J. Hydrol.*, **88**, 147–164 (1986).

80. J. W. Jones, "Long-term and higher temporal resolution river reach width estimation through the assembly of multi-spatial, -spectral, and -temporal resolution databases: experience from an Alaska Pilot Study," in *AGU Fall Meeting*, Washington, D.C. (2018).
81. G. J. Arcement and V. R. Schneider, *Guide for Selecting Manning's Roughness Coefficients for Natural Channels and Flood Plains*, Water-Supply Paper 2339, USGS (1989).
82. S. E. Yochum, "Flow resistance coefficient selection in natural channels: a spreadsheet tool," USDA FS Technical Summary TS-103.2 (2018).
83. J. Falcone, "GAGES-II: geospatial attributes of gages for evaluating streamflow [Dataset]," U.S. Geological Series Report, 2011, https://water.usgs.gov/GIS/metadata/usgswrd/XML/gagesII_Sept2011.xml#stdorder (accessed 31 May 2022).
84. D. M. Wolock, "Baseflow index grid for the conterminous United States [Dataset]," U.S. Geological Survey Open-File Report, 03-263, 2003, https://water.usgs.gov/GIS/metadata/usgswrd/XML/bfi48grd.xml (accessed 31 May 2022).
85. D. Mazvimavi, A. M. J. Meijerink, and A. Stein, "Prediction of baseflows from basin characteristics: a case study from Zimbabwe/Prévision de débits de base à partir de caractéristiques du bassin: une étude de cas au Zimbabwe," *Hydrol. Sci. J.* **49**(4), 703–715 (2004).
86. C. A. Rumsey et al., "Regional scale estimates of baseflow and factors influencing baseflow in the Upper Colorado River Basin," *J. Hydrol.: Reg. Stud.* **4**, 91–107 (2015).
87. United States Geological Survey (USGS), "National map data delivery GIS data download," https://www.usgs.gov/the-national-map-data-delivery/gis-data-download (accessed June 2022).
88. S. E. Rantz, *Measurement and Computation of Streamflow: Volume 1 Measurement of Stage and Discharge*, Water Supply Paper 2175, p. 284, U.S. Geological Survey (1982).
89. F. M. Henderson, *Open Channel Flow*, 522 p., Macmillan, New York (1966).
90. A. H. Shapiro, Shape and Flow: The Fluid Dynamics of Drag, pp. 186, Doubleday & Co., Garden City, New York (1961).
91. National Aeronautics and Space Administration (NASA), Earth Science Applied Sciences, *Water Resources Enhancing Water Management*, https://c3.nasa.gov/water/projects (accessed June 2022).

Biographies of the authors are not available.